NOTICE

The quality of this microform is heavily dependent upon the quality of the original thesis submitted for microfilming. Every effort has been made to ensure the highest quality of reproduction possible.

If pages are missing, contact the university which granted the degree.

Some pages may have indistinct print especially if the original pages were typed with a poor typewriter ribbon or if the university sent us an inferior photocopy.

Previously copyrighted materials (journal articles, published tests, etc.) are not filmed.

Reproduction in full or in part of this microform is governed by the Canadian Copyright Act, R.S.C. 1970, c. C-30.

AVIS

La qualité de cette microforme dépend grandement de la qualité de la thèse soumise au microfilmage. Nous avons tout fait pour assurer une qualité supérieure de reproduction.

S'il manque des pages, veuillez communiquer avec l'université qui a conféré le grade.

La qualité d'impression de certaines pages peut laisser à désirer, surtout si les pages originales ont été dactylographiées à l'aide d'un ruban usé ou si l'université nous a fait parvenir une photocopie de qualité inférieure.

Les documents qui font déjà l'objet d'un droit d'auteur (articles de revue, tests publiés, etc.) ne sont pas microfilmés.

La reproduction, même partielle, de cette microforme est soumise à la Loi canadienne sur le droit d'auteur, SRC 1970, c. C-30.

SOME PROPERTIES OF THE SEMIMAGNETIC-SEMICONDUCTOR ALLOY SYSTEM $Cd_{2x}(AgGa)_yMn_{2z}Te_2$

By

Munkith I. Al-Najjar

Thesis submitted to the
School of Graduate Studies
in partial fulfillment of the requirements
for the degree of
Master of Science in Physics

Department of Physics
Faculty of Science
University of Ottawa
Ottawa, Ontario

1987

ISBN 0-315-40680-1

UNIVERSITÉ D'OTTAWA
UNIVERSITY OF OTTAWA

ABSTRACT

This thesis deals with the subject of exchange interaction and the magnetic ordering in the alloy system $Cd_{2x}(AgGa)_yMn_{2z}Te_2$ (x+y+z=1). This alloy system belongs to the class of materials known as semimagnetic-semiconductors (SMSC), also known as diluted magnetic semicondutors (DMS), in which an ordinary semiconductor is alloyed with a magnetic semiconductor resulting in a random distribution of the magnetic ions on the lattice sites. The introduction of magnetic ions into the semiconductor results in anomalous effect in the magnetic and the magneto-optical properties of these materials.

Samples were grown in the polycrystalline form using the standard method of melt and anneal. Investigations of the lattice structure, magnetic susceptibility, ESR linewidth and energy gap were then carried out as a function of sample composition, and especially as a function of the manganese concentration.

Magnetic susceptibility measurements showed a spin glass like behavior in this alloy system, where the spins become locked in a random configuration in the lattice at certain temperature T_g (freezing temperature). However, the spins in some samples of this system showed an antiferromagnetic behavior characterized by a critical temperature T_N (the Néel temperature), due to the ordering of the magnetic ions on the lattice sites. The model of superexchange proposed by Geertsma et al, describes the interactions between the magnetic ions in these materials as taking place via virtual transitions between the valence band and the energy levels of the magnetic ions (the $3d^5$ levels of the Mn^{2+} ions in our alloy system). The introduction of this model into our alloy system resulted in a reasonable agreement between the calculated values of the Curie-Weiss temperature and the experimentally acquired ones.

Measurements of the width of the ESR absorption line was performed as a function of

temperature and of composition. From these measurements, information regarding the presence of the ordered or the disordered state of the spins was obtained, as well as the dependence of such presence on the method of heat treatment followed in the growth of the samples. From the analysis of the ESR lines, values of the Curie-Weiss temperature could be predicted and found to be in good agreement with those obtained from the magnetic susceptibility measurements.

An optical absorption technique was used to determine the energy gap value of these materials. Allthough only few of such values could be determined, due to difficulties in the sample preparation, it was found that the energy gap value of the sample depends on whether the spins are in an ordered or disordered configuration in the lattice.

ACKNOWLEDGEMENTS

I would like to thank my supervisor Dr. G. Lamarche for his advice and assistance during this research and the writing of this thesis.

I would like to express my gratitude to Dr. J.C. Woolley for very helpful discussions and for his unique comments during the writing of this thesis. I also would like to thank Dr. A. Manoogian for the discussions and the assistance in the ESR measurements.

I wish to thank Dr. T. Donofrio for friendship and for valuable discussions and for the assistance he provided in explaining some computer techniques. I would also like to thank Dr. S. Chehab, Dr. M. Quintero and L. Dierker for their help and discussions. I wish to express my gratitude to Mr. B.W. Chan for friendship and patience in providing the ESR measurements. Also my thanks to Mr. R. Chagnon for his assistance in the use of the computer facility during the preparation of this thesis.

I extend my gratitude to my family - most of all, my wife Shirley for her patience and emotional support, and also to my mother and my brother Nabil for their love and support.

TABLE OF CONTENTS

LIST OF FIGURES

LIST OF TABLES

CHAPTER 1
INTRODUCTION

There has been a considerable amount of interest in Semimagnetic-Semiconductors (SMSC) in recent years. The name SMSC (or diluted magnetic semiconductors (DMS)) refers to a class of materials intermediate between magnetic and non-magnetic semiconductors.

Such type of materials can be obtained by alloying an ordinary semiconductor with a magnetic semiconductor, i.e. by substituting a paramagnetic ion on the cation sublattice of a compound semiconductor. The presence of such ions causes differences in the semiconductor's properties. This change in the properties of the semiconductor includes giant magneto-optical effects and enhanced Zeeman splitting of the band, magnetic field dependence of the acceptor activation energy and most importantly the spin glass behavior exhibited by these materials. If the alloy so produced is to be a semiconductor, then the electron to atom ratio must be conserved; i.e. on the average, the magnetic ions must replace non-magnetic cations of the same valency.

Most of the work on such class of alloys (1,2) has been concerned with replacing the divalent elements Zn, Cd and Hg by manganese ions, eg. $Cd_{1-z}Mn_z$ Te. It is possible, however, to produce similar alloys from the chalcopyrite I III VI_2 compounds, the ternary analog of the II VI compounds. If the paramagnetic ion to be included in these materials is Mn^{2+}, then in order to retain the electron to atom ratio, it is necessary to replace one I and one III cation simultaneously by two manganese atoms, giving alloys of the form $(I\ III)_{1-z}Mn_zTe_2$ with I being Cu or Ag and III being Ga or In. The most interesting aspect of these mixed crystals is the presence of the half-filled $3d^5$ levels of the manganese ions. The localized magnetic moments of the $3d^5$ electrons interact with each other as well as with the band electrons via exchange interaction, giving rise to anomalous magnetic and magneto-optical effects, eg. giant Faraday rotation and the Zeeman splitting of the band (3).

In this thesis, the investigations of some of the properties of the pseudo-ternary alloy system $Cd_{2x}(AgGa)_y\ Mn_{2z}\ Te_2$ (x+y+z=1) are presented. This work is part of the investigation of the properties of similar alloy systems of the form $II_{2x}(I\ III)_yMn_{2z}Te_2$, such as:

$Cd_{2x}(Cu\ In)_y\ Mn_{2z}Te_2$

$Cd_{2x}(Ag\ In)_y\ Mn_{2z}Te_2$

$Zn_{2x}\ (Cu\ In)_y\ Mn_{2z}Te_2$

$Cd_{2x}(Cu\ Ga)_y\ Mn_{2z}Te_2$

performed by our research group. The composition of samples grown in this work can be represented by a triangle, figure (1.1), where each point in the triangle represents a certain value of x,y and z.

Polycrystalline samples were grown by the standard method of melt and anneal described in chapter (2). The alloys were grown in this polycrystalline form instead of single crystals due to the fact that a large number of samples was required in order to study the dependence of several of the properties of the alloy system on composition. The results obtained in the case of other similar systems grown in polycrystalline form by other members of the research group, such as $Cd_xZn_yMn_zTe$ (4) and $Cd_xHg_yMn_zTe$ (5); did not show significant differences from those obtained from single crystals studied by other research groups.

The various properties of our alloy system were investigated by studying

1- Variation of the lattice parameter with composition using the powder x-ray diffraction technique (chapter 2).

2- The samples' magnetic behavior by measuring its low field magnetic susceptibility as a function of temperature and manganese concentration (chapter 3).

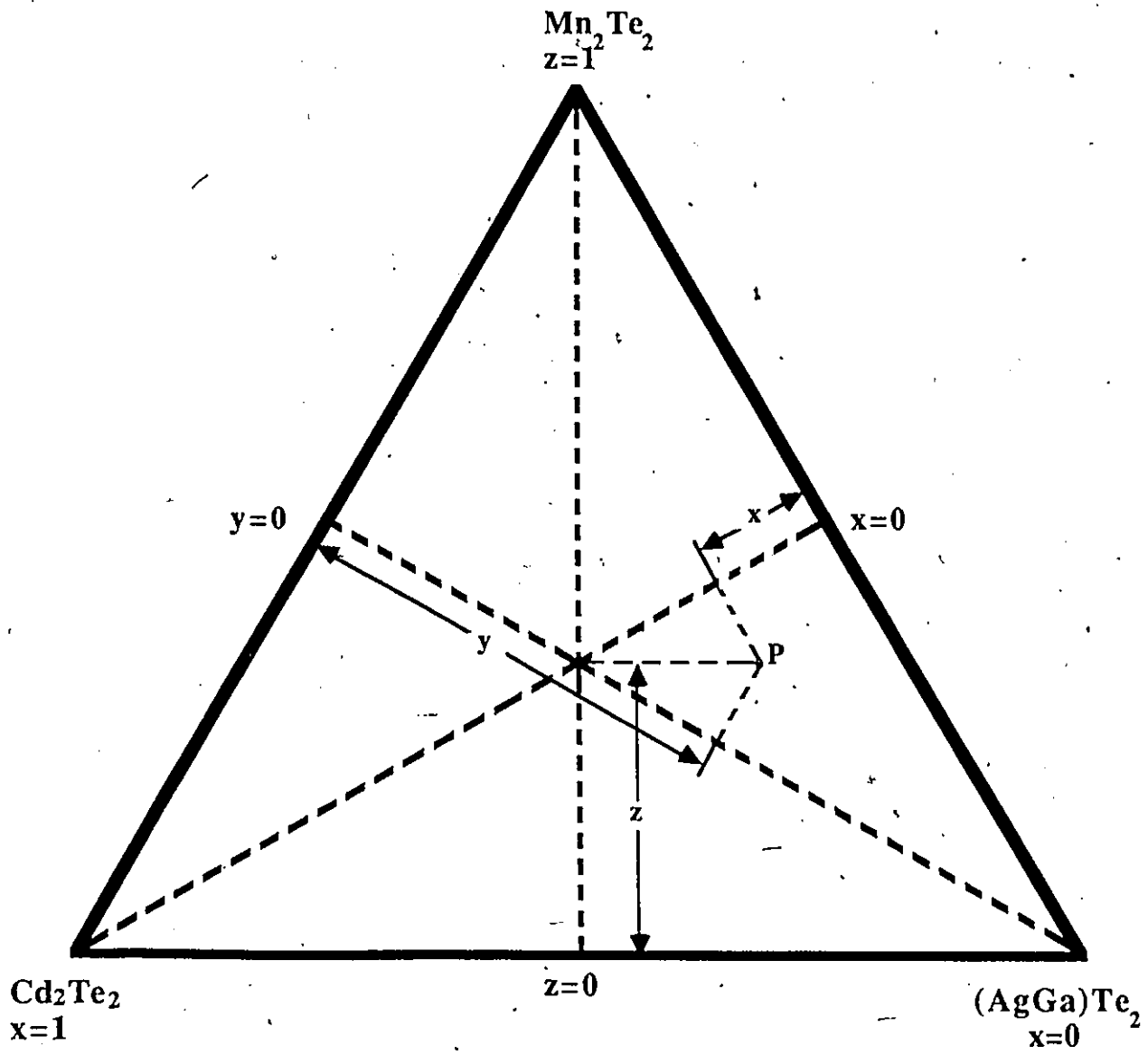

Figure 1.1 Triangular Coordinate System.
Any point 'P' in the diagram represents a sample of composition (x, y, z).

3- Variation of the linewidth of the absorption line in Electron Spin Resonance (ESR) measurements with temperature and sample composition (chapter 4).

4- Determination of some of the samples' energy gap values as a function of composition using optical absorption method (chapter 5).

CHAPTER 2
X-RAY MEASUREMENTS

2.1 INTRODUCTION

Polycrystalline samples of the alloy system $Cd_{2x}(AgGa)_yMn_{2z}Te_2$ were made by the standard method of melting and annealing described in the following section. The exact procedure followed in the heat treatment of the ingot was found to affect the magnetic and optical properties of the sample. The method of x-ray powder diffraction photography was used to determine the condition of the samples prior to performing the magnetic susceptibility, Electron Spin Resonance and optical energy gap measurements. Only samples that were found to be in equilibrium and homogeneous, when studied by this method, have been considered in these measurements. Also the analysis of these photographs provided information about the general phase diagram of this alloy system.

2.2 SAMPLE PREPARATION

The preparation method of polycrystalline samples is similar to that used by T. Donofrio (4). The components of each sample were weighed to an accuracy of .0001 gm, and a total sample of 1 gm was prepared in order to have enough material to perform the various types of measurements. The components were then sealed in a quartz tube under vacuum ($5 * 10^{-5}$ mm.Hg). The quartz tube had to be carbonized in order to prevent the manganese from attacking the quartz and exploding at high temperatures during the melting process. The procedure of carbonizing the tubes is as follows: the empty quartz tube was first closed at one end by melting the quartz using an oxygen acethylene torch. This end was then rounded by further heating in order to prevent the occurrence of thin areas that might lead to an explosion at high temperatures.

The quartz tube was then flushed with acetone and emptied carefully so that no drops of acetone remained inside. The tube was then gradually heated with the torch in order to leave a layer of carbon on the interior walls of the tubes. The quality of the carbon layer was verified in all prepared tubes, by exposing the tube to a strong source of light. If the carbon layer had any spots where light could get through, the carbonizing procedure was repeated. The maximum temperature that could be obtained in the melting furnace was 1100 ^{o}C, which is lower than the melting temperature of manganese (table 2.1); however, the manganese dissolves with the other components.

Element	Melting point (^{o}C)
Cd	321.03
Ag	960.8
Ga	29.78
Mn	1244 ±3
Te	449.5

Table (2.1) melting points of elements

The maximum temperature was reached in approximately 6 hours in the melting furnace. The sample was then left at that temperature in the furnace for one half hour while being periodically shaken to ensure a thorough melting of all components. Then the furnace was turned off and the sample was left in it to cool slowly over several hours.

Afterwards, the samples were placed in another furnace in order to anneal at

650 ±10 °C for three weeks or longer. With this heat treatment, samples were found to achieve satisfactory equilibrium and homogeneity conditions as observed in the analysis of the x-ray powder diffraction photographs for several portions of the specimen.

It was found that the sample's magnetic and optical properties, in almost all cases, were strongly influenced by the procedure followed in cooling the material from the annealing temperature. It is proposed that this type of dependence on the heat treatment is due to the possible ordering of the manganese atoms in the lattice. Some evidence of such ordering could be concluded from the analysis of the magnetic and optical properties of these materials discussed in following chapters. As a result of this, two types of cooling procedure from the annealing temperature were followed. To obtain a high degree of ordering in the material the sample was cooled slowly in the furnace. In this case the material spends sufficient time in the ordering region during the cooling process below the annealing temperature. Only partial ordering, however, is achieved in this method as observed in magnetic susceptibility and ESR measurement. The reason for not achieving complete ordering in the samples is our lack of knowledge of the exact ordering temperature of each sample. This information is now being sought by another student. The second procedure consists of the rapid quenching of the sample by immersing it in water in order to obtain as little ordering as possible. Thus, the material is not allowed to remain in the ordering region for any length of time. Unfortunately this procedure did not provide complete absence of the ordering because of the insufficient speed of the temperature drop.

2.3 ZINC-BLENDE AND CHALCOPYRITE STRUCTURES

The zinc-blende and the chalcopyrite structures are derived from the tetrahedrally bonded diamond structure, and called adamantine structures. There are two basic conditions to be satisfied in both cases, namely, having an average of four valence electrons per lattice site, and an equal

number of anions and cations.

The II-VI materials have a zinc-blende lattice structure derived from that of diamond in such a way that one of the fcc sublattices is occupied by the anion (VI) and the other by a combination of group VI elements, with an average of four valence electrons per lattice site. The structure of the zinc-blende lattice and a projection of the atomic positions are depicted in figure (2.1). In this structure, atoms of the group II are bonded tetrahedrally to the group VI atoms that are displaced by a/4 along the face diagonal. The difference between the zinc-blende and the diamond lattices is that the symmetry of zinc-blende is reduced because of the ordering of the two different types of atoms, while the diamond structure consists of identical atoms which leads to a higher symmetry.

Materials of the type I- III-VI_2 have a $GuFeS_2$ chalcopyrite lattice structure which is derived from the diamond lattice. These materials have a body centered tetragonal lattice where c/a is equal or slightly less than 2, with its unit cell containing 16 atoms. In this structure the two types of cations occupy two different sublattices, figure (2.2), while the anions occupy another sublattice. In this structure atoms of the groups I and III are tetrahedrally coordinated by four VI atoms; where each of the VI atoms is coordinated by two atoms of each of the I and III (6).

2.4 X-RAY RESULTS AND ANALYSIS

Debye-Scherrer photographs were taken for samples of the alloy system $Cd_{2x}(AgGa)_y$ $Mn_{2z}Te_2$ over the range of composition shown in figure (2.3). These photographs were used, first, to verify if the sample had reached its equilibrium condition after the heat treatment. The actual analysis of these photographs, which will be described shortly, was used to determine the crystal structure and the lattice parameter of each sample. Absorption by the sample's holder had to be taken into consideration, in order to determine the real Bragg angle of reflection. For this

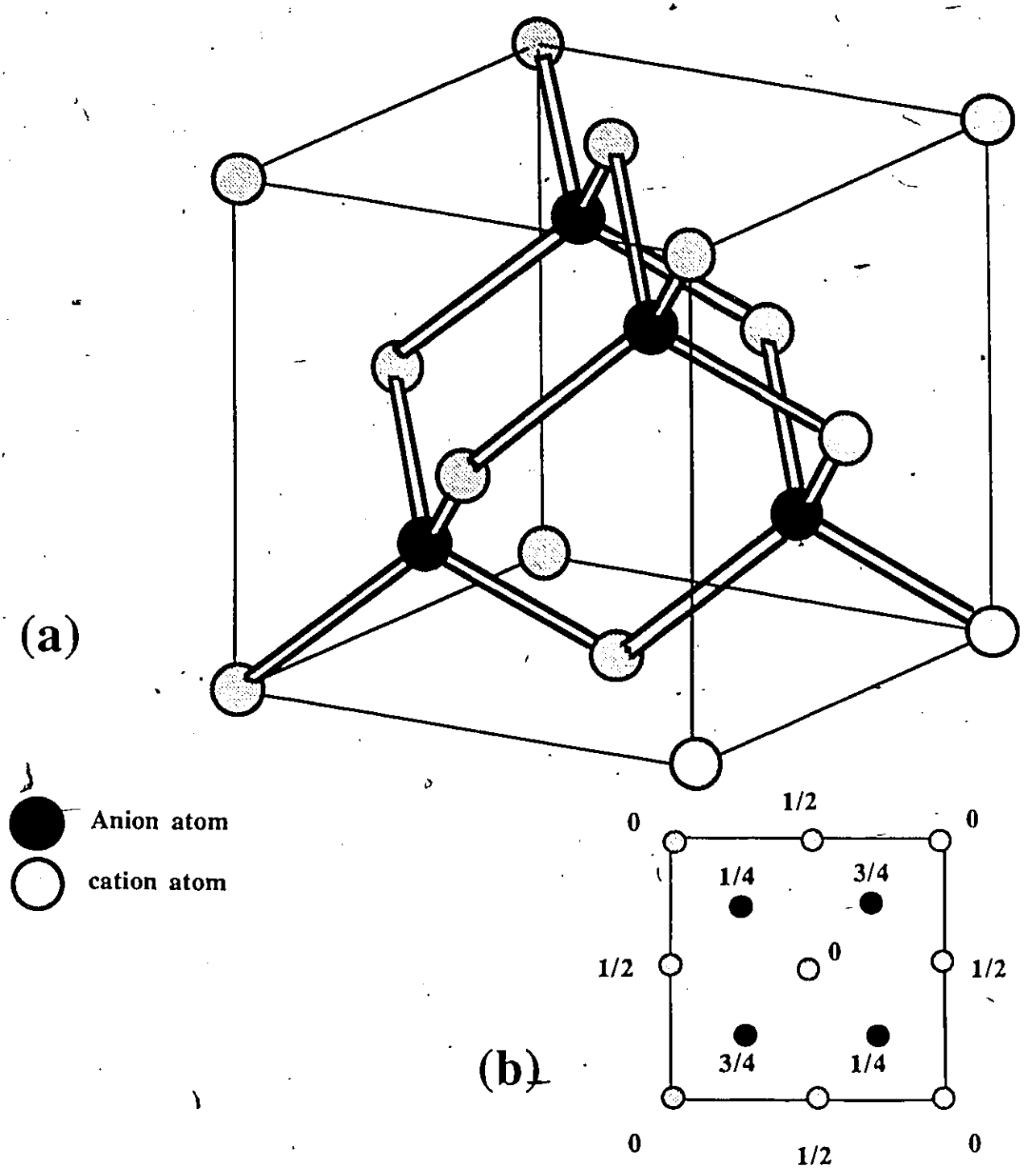

Figure 2.1 a) zinc-blende structure
b) projection of atomic positions on the c-face.

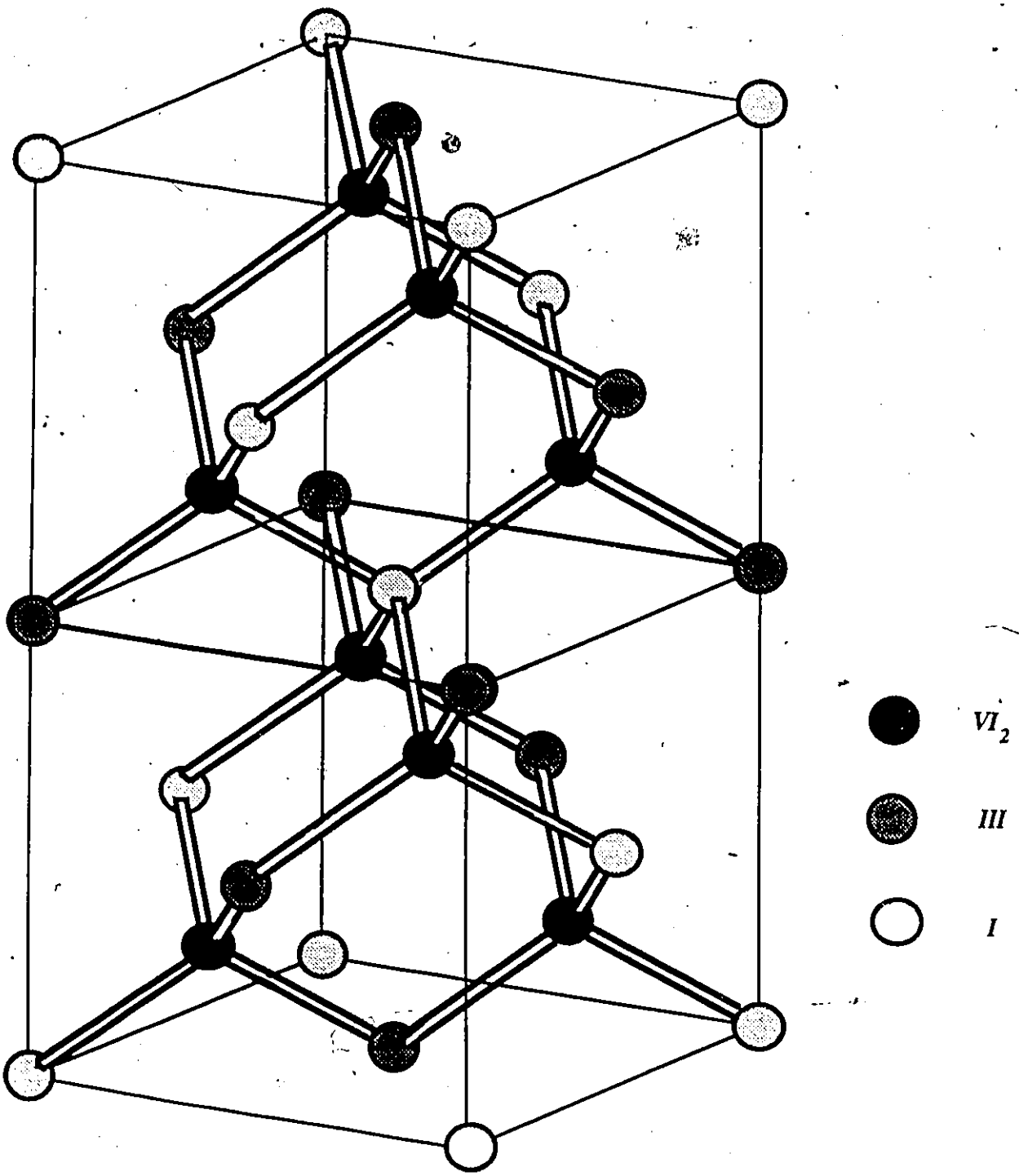

Figure 2.2 Chalcopyrite lattice

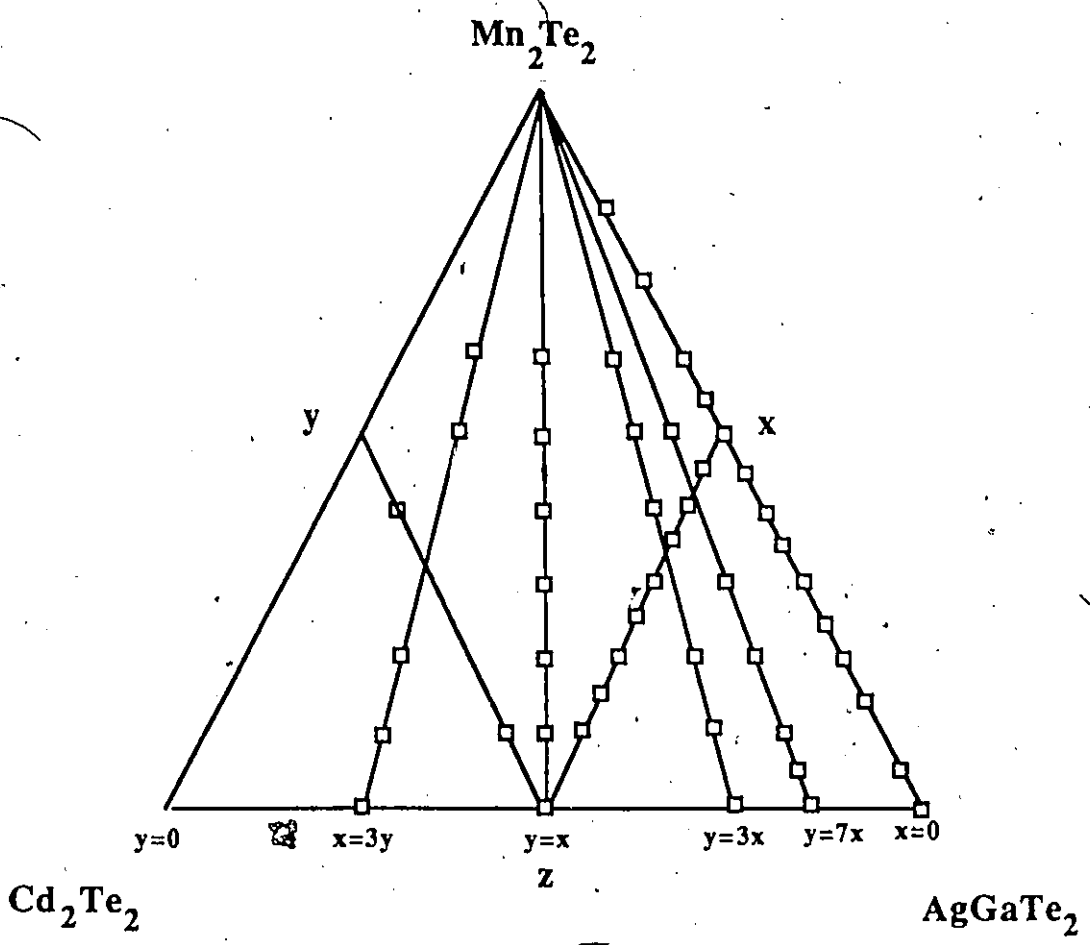

Figure 2.3 **Range of composition in triangular coordinates for samples studied by x-ray photography.**

purpose two correction methods were used. In the case of zinc blende samples the values of lattice parameter obtained from the observed lines were plotted against a correction function f(θ) (Nelson-Riley correction function) given by the following expression:

$$f(\theta) = \frac{\cos^2(\theta)}{2\sin(\theta)} + \frac{\sin^2(\theta)}{2\theta} \qquad (2.1)$$

where θ is the Bragg angle. This function is chosen to have this form in order to give a linear relation between the lattice parameter "a" and θ, figure (2.4). The best straight line is drawn through the points, and the correct value of "a" is obtained by extrapolating to f(θ)=0.

In the case of samples in the chalcopyrite region (body centered tetragonal structure with c/a ≠2) the application of the correction method discussed above was found to be lengthy and tedious. In this case, a plot of the variation of the two parameters (c and a) with f(θ) had to be made in order to obtain the corrected values of the lattice parameters from the intersections of the extrapolated lines with the y-axis at f(90). In order to get a good correction, one has to adjust these two lines until they become parallel, which indicates that the two parameters are affected by an equal amount of absorption.

Therefore, the method of internal calibration was used instead. This method involves mixing a small amount of silicon (which has a well known value of lattice parameter) with the sample being x-rayed. From the analysis of the silicon lines, a correction graph of $\sin^2(\theta)$ versus $\Delta\sin^2(\theta)$ was plotted, where $\Delta\sin^2(\theta)$ is the difference between the squared sine of the measured and the standard Bragg angle of reflection of the silicon. From this graph, the values of $\sin^2(\theta)$ for the chalcopyrite sample were interpolated to determine the values of $\Delta\sin^2(\theta)$ which represent the correction to be made on the observed values of $\sin^2(\theta)$. Since the conditions under which the x-ray photographs were taken were very similar (such as the length and the thickness of the

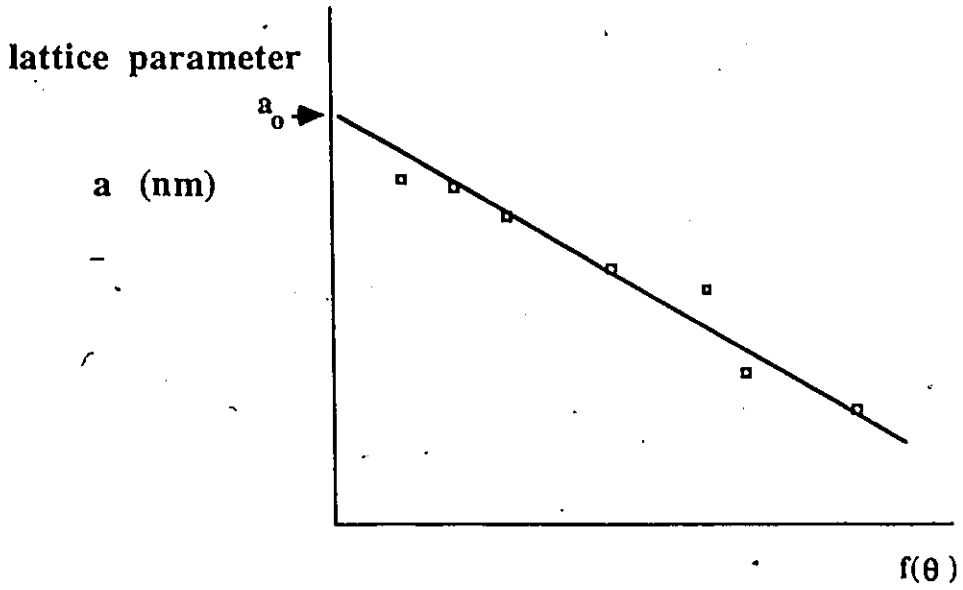

Figure 2.4 Variation of lattice parameter with f(θ), representing the effect of absorption on lattice parameter.

holder), this correction method was obtained for one of the chalcopyrite samples, and then used in the analysis of all the other chalcopyrite samples. This approximation is justified since the error involved in accepting such small differences in the method of taking these photographs is negligible in comparison with the errors introduced in the determination of the position of the lines on the x-ray film and in our knowledge of the exact sample composition after the melting and annealing stages.

The lattice parameter was determined from the x-ray photographs using the Bragg condition of reflection, equation (2.2),

$$\sin^2(\theta) = N \frac{\lambda^2}{4\,a^2} \qquad (2.2)$$

where

$$N = h^2 + k^2 + l^2$$

λ: wavelenght of incident x-ray radiation

θ: Bragg angle of reflection

a: lattice parameter

h, k, l: Miller indices

In fcc structure, which is the case of zinc-blende, the Miller indices (h,k,l) have to satisfy the condition of being all odd or all even (see table 2.2) and such that:

$h+k+l = 4n$

$h+k+l = 4n+2$

$h+k+l = 2n+1$

where n is an integer.

The angle of reflection (θ) was measured for each line, and then the predicted values of

the Miller indices (hkl) of the lines were fitted to equation (2.2) in order to obtain a smooth variation between "a" and f(θ), as discussed earlier. In the case of chalcopyrite samples, the Bragg condition is

$$\sin^2(\theta) = \lambda^2 \left[\frac{h^2 + k^2}{4a^2} + \frac{l^2}{4c^2} \right] \qquad (2.3)$$

where the Miller indices can be derived from the zinc-blende indices by doubling the l index (see table 2.2). A computer program was designed to perform the fitting of the Miller indices to the observed value of $\sin^2(\theta)$, after being corrected using the internal calibration method described above. The first step in this program is to predict the Miller indices for as many of the observed lines as possible. This is accomplished by assigning the values of (hkl) to these lines according to table (2.2) and then using these values to calculate the corresponding line positions. This is tried several times until the predicted line positions are in good agreement with the observed ones. Once the Miller indices for the first few lines are determined, the Bragg equation is then solved for "a" and "c" using a least square fit. These values were then used to determine the values of the (hkl) indices for the rest of the observed lines, by comparing their calculated line positions with the observed ones. Having assigned the correct (hkl) values to all of the lines, the Bragg equation is then solved for all the lines in order to obtain a precise value for "a" and "c" by using a least square fit.

The values of lattice parameter are plotted against the Mn^{2+} concentration (z) in figures (2.5) and (2.6). The variation of "a" with "z" was found to be linear over the studied range of composition. Each line in these two plots represents certain ratio of x/y. The values of lattice parameter for samples with y=0 were obtained from the work of T. Donofrio on the system

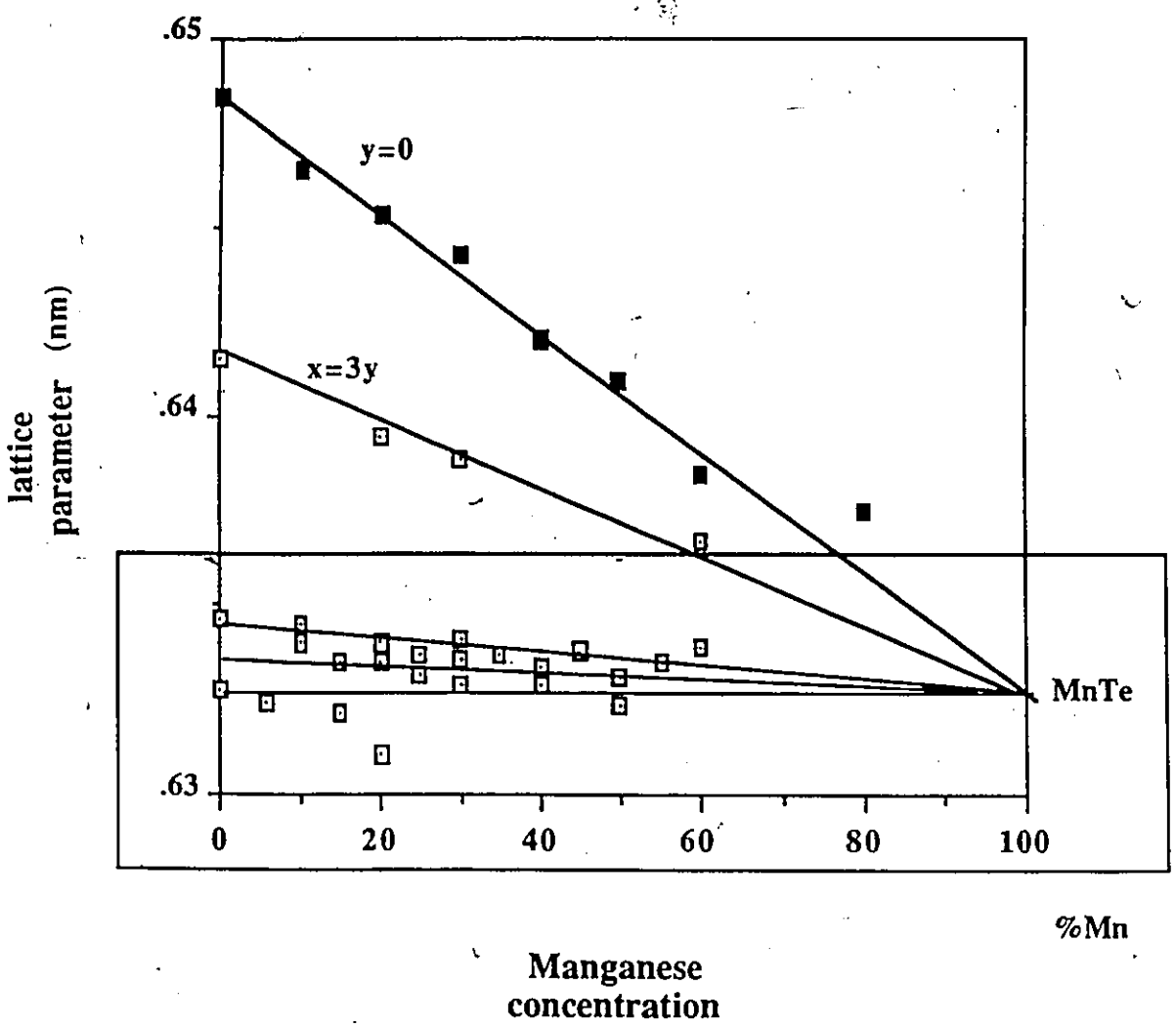

Figure 2.5 Variation of lattice parameter with manganese concentration. Area enclosed in rectangle is shown in figure 2.6.

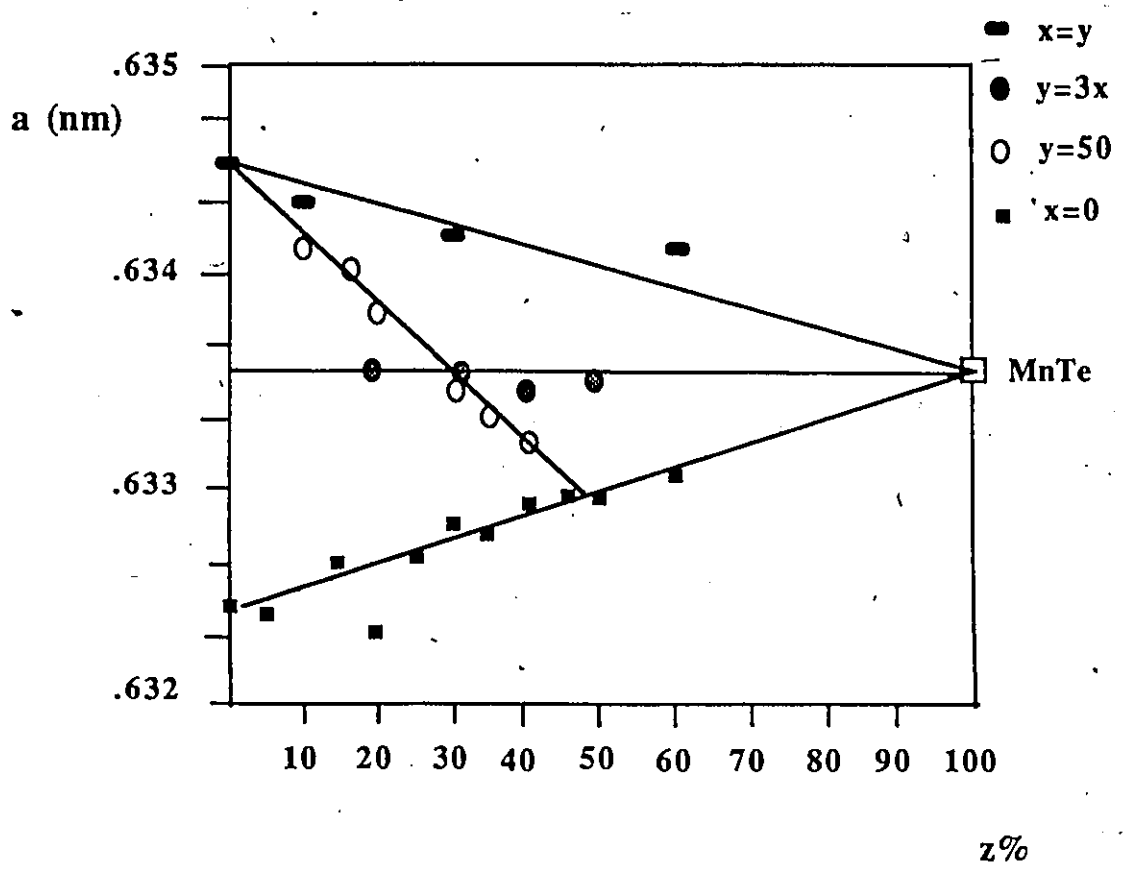

Figure 2.6 Lattice parameter variation with Mn concentration.

$Cd_xZn_yMn_zTe$ (4). Figure (2.7) represents an isothermal section of the phase diagram at T=650 °C for the alloy system $Cd_{2x}(AgGa)_yMn_{2z}Te_2$ in triangular coordinates, showing the range of solid solution and the approximate border lines between the phase regions. The lines drawn in this diagram are the approximate boundaries of the phases according to the calculated values of lattice parameter. A detailed and precise determination of these boundaries requires a considerable amount of additional work, which is outside the scope of this thesis.

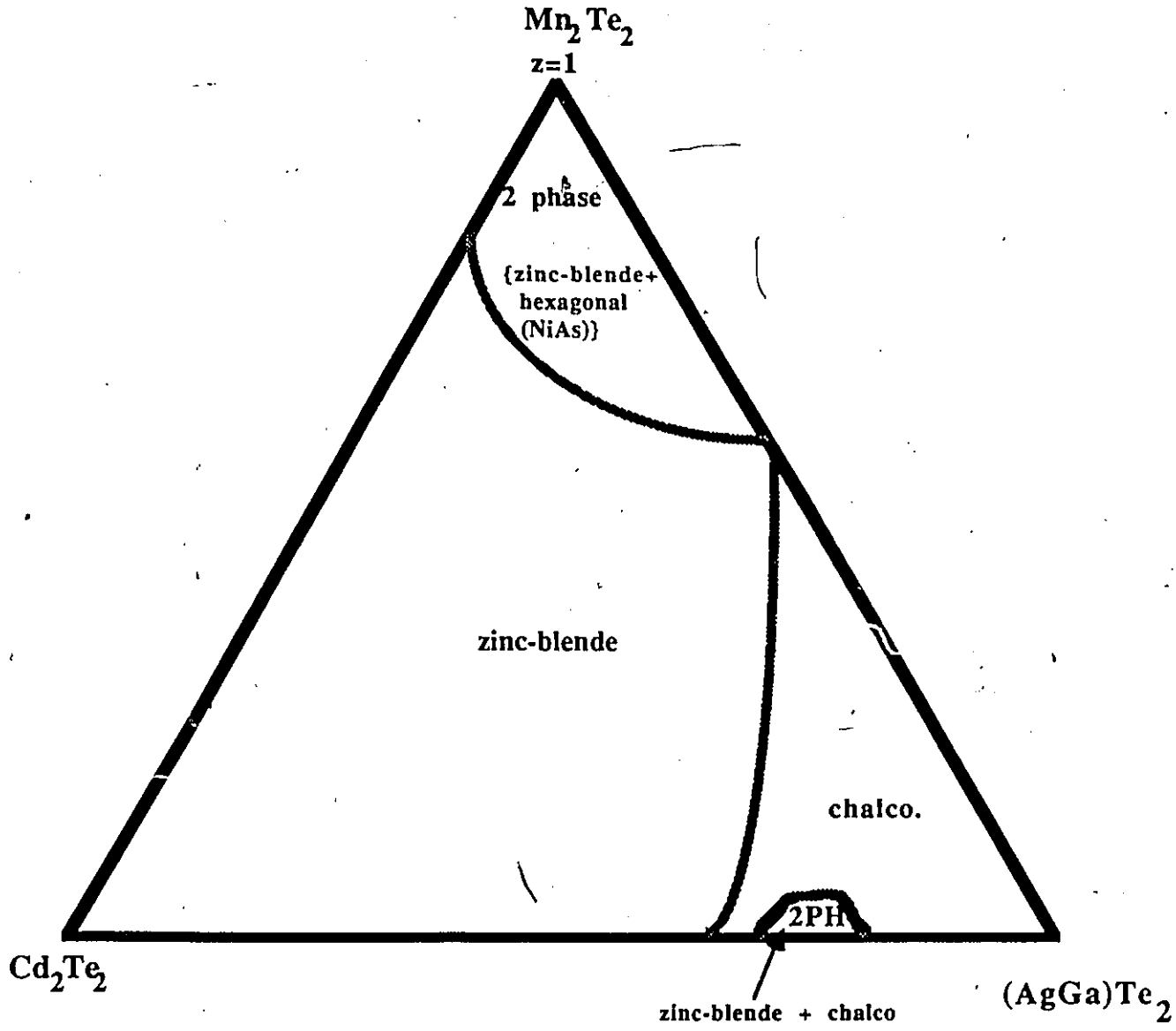

Figure 2.7 Phase diagram showing range of solid solution and approximate border lines between the phase regions.

N	zinc-blende	chalcopyrite
	hkl	hkl
3	111	112
4	200	200
		004
8	220	220
		204
11	311	312
		116
12	222	224
16	400	400
		008
19	331	332
		316
20	420	420
		404
		208
24	422	424
27	511	512
	333	336
		1110
32	440	440
		408
35	531	532
		516
		3110
36	600	600
		0012
40	620	620
		604
		2012
43	533	536
		3310
44	622	624
		2212

Table 2.2 Values of Miller indices for zinc-blende and chalcopyrite structures.

CHAPTER 3
MEASUREMENTS OF MAGNETIC SUSCEPTIBILITY

3.1 INTRODUCTION

Semimagnetic-Semiconductors (SMSC) or Diluted Magnetic Semiconductors (DMS) in which the magnetic ions such as Mn^{2+} assume random positions in the lattice, show an unmistakable cusp in their magnetic susceptibility versus temperature behavior. The sharp cusp observed in these materials is attributed to the freezing of magnetic ions in random orientations. This interpretation is supported by neutron diffraction measurements which also indicate the absence of any long range ordering of the magnetic ions at and below the freezing temperature of the spins T_g. On the other hand, no corresponding anomaly was observed in the specific heat measurements, raising as yet unanswered questions regarding the nature of such a freezing process.

In the diluted magnetic semiconductor alloy system $Cd_{2x}(AgGa)_y\ Mn_{2z}Te_2$, the magnetic susceptibility measurements above 4.2 K exhibit this typical behavior of spin glass freezing for samples with manganese concentration ranging between 15% to ~55% . These measurements showed that the magnetic behavior of the alloys is different for different types of structures in which they crystallize, zinc-blende and chalcopyrite. This is due to the effect of the structure of the lattice on the exchange interaction between the spins. Such a difference is rendered more complicated in these materials due to the presence of different possible types of ordering of the manganese ions in each of the structures of the material. Investigation of the freezing temperature T_g and of the Curie-Weiss temperature (θ), were carried out in order to obtain information about the nature of the exchange interaction between neighboring Mn^{2+} ions, as well as the value of the exchange integral (J). The apparatus used for this purpose , discussed later in this chapter, is the SQUID magnetometer designed and built by Professor G. Lamarche in the low

temperature physics laboratory at the University of Ottawa.

3.2 THEORETICAL BACKGROUND

The name "spin glass" was first introduced by B. Coles (7) to denote "the entire class of random magnetic alloys of moderate dilution in which the magnetic structure no longer resembles that of pure metals ". Another definition was given by Binder (8) who describes a spin glass as a "magnetic system where the interaction between the spins are in conflict with each other, due to 'quenched (i.e. frozen-in) disorder' in the system". The reason for calling these materials glasses is that in ordinary glasses, the spatial degrees of freedom freeze without any long-range order similar to the absence of the long-range order in the freezing of spins in these materials (9).

In the case of metallic spin glass materials, the RKKY (Ruderman-Kittel-Kasuya-Yosida) model, which represents an indirect coupling of the spins via the conduction electrons, is the dominant mechanism of interaction which leads to the spin freezing. This interaction oscillates between decaying positive and negative values as the distance between nearest neighbors increases (10). This type of interaction is insignificant in some SMSC, including the alloy system under study, which have a low carrier concentration.

Lattice frustration is believed to be the origin of the random freezing phenomenon in spin glasses. This frustration arises in these materials due to a contradiction of interaction. In metallic spin glasses, where the RKKY is dominant, the influence of magnetic interaction on any site (i) by other sites could be in conflict, leading to frustration. In a zinc-blende or a chalcopyrite structure, where the spins tend to align antiferromagnetically, frustration may arise due to the geometrical arrangement of the spins. In such case, a spin that tends to be aligned in a certain direction due to the influence of a nearest neighbor could be acted upon by another nearest neighbor in an opposite direction. The resulting situation represents an equilibrium position of the spin leading to the random freezing in a three dimensional lattice. Frustration may arise only from nearest neighbors

antiferromagnetic interaction and not necessarily from a competition between ferromagnetic and antiferromagnetic interactions (9). In the case of the zinc-blende structure for example, the frustration arises as shown in figure (3.1), where any of the spins in the triangle will be frustrated due to the competing influences of the other two spins.

It has been suggested for the case of metallic spin glasses (11,12) that the freezing process in these materials is a gradual one similar to the blocking of superparamagnetic single domain magnetic particles. Thus, for a particular measurement, these single domain particles will appear to be frozen if their relaxation time is larger than the measurement time of the experiment, (the interval of time during which the experiment probes the system). This model succeeds in explaining the dependence of the a.c. magnetic susceptibility measurements on the frequency of the oscillating magnetic field, as well as the difference in the value of the freezing temperature (blocking temperature) obtained by a.c. susceptibility, by neutron diffraction (13) and by Mossbaüer effect (14). The difference between these measurements is attributed to the difference in the measurement time of these experiments.

However, in insulating spin glasses, such as $Cd_{2x}(AgGa)_yMn_{2z}Te_2$, the interaction between the spins is found to be antiferromagnetic from the study of the Curie-Weiss temperature. Thus, clustering in these materials is different from that in metallic spin glasses. At high temperature the interaction between spins is weak which results in a paramagnetic behavior of the susceptibility according to Curie-Weiss theory of antiferromagnetism. This behavior is represented by the linear relationship between $1/\chi$ and T as shown in figure (3.2). At lower temperatures, small clusters start to form in which the spins tend to align antiferromagnetically for longer intervals of time due to an increase in the correlation time between them. The superparamagnetism arises in this case from unpaired spins on the surface of the cluster resulting in large net magnetic moment (15). This enhanced paramagnetic behavior could also be attributed, in part, to the isolated spins which are not included in any one of the clusters. As the temperature is

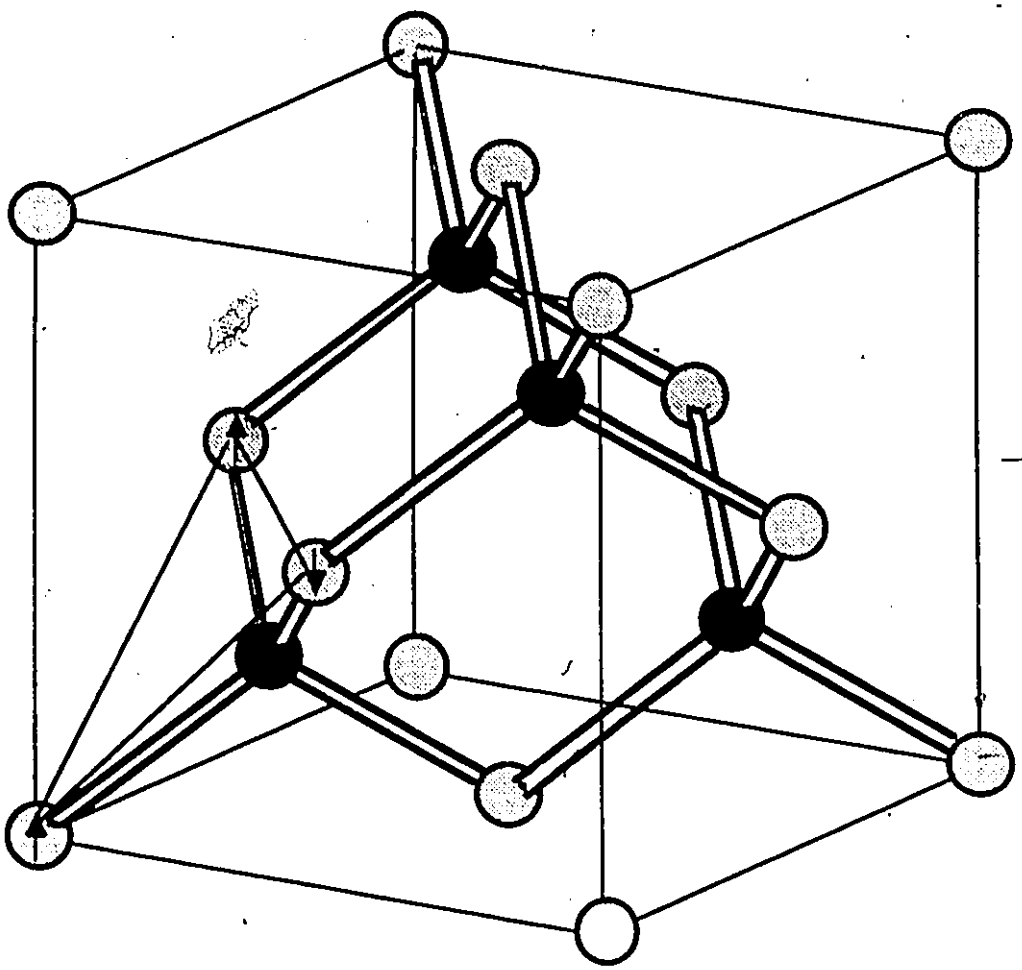

Figure 3.1 Frustration in a zinc-blende lattice.

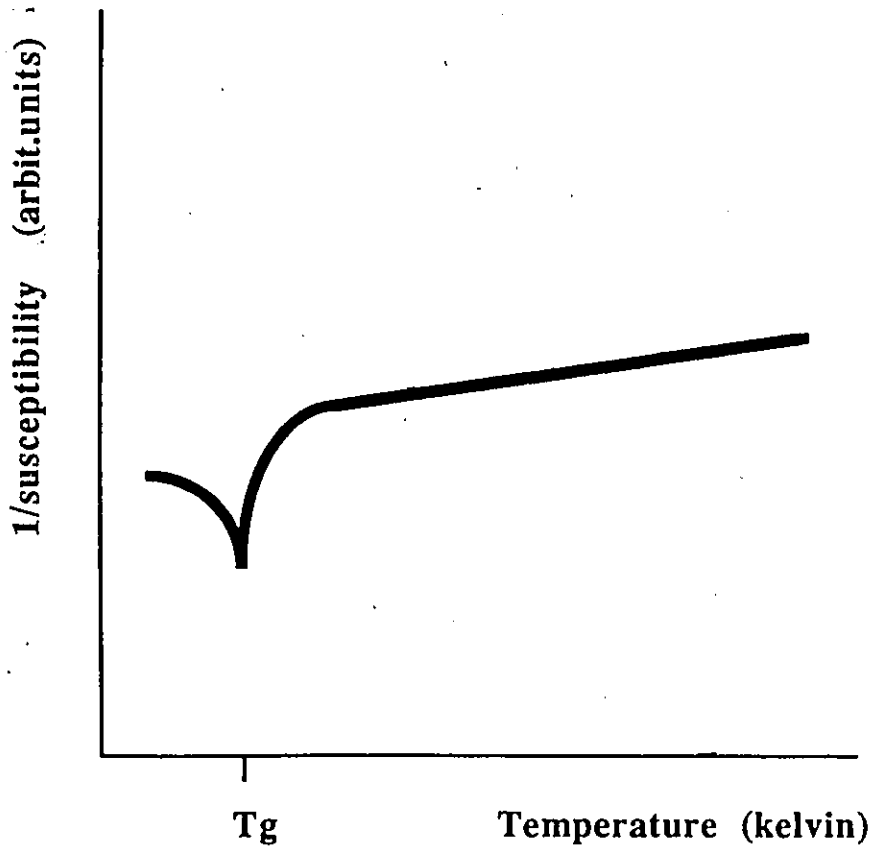

Figure 3.2 Typical variation of the inverse of magnetic susceptibility with temperature.

lowered further, more and more loose spins will join the clusters until an infinitely large cluster forms at some critical temperature Tg, the freezing temperature.

As to the nature of the exchange mechanism responsible for the observed antiferromagnetism, the direct type of exchange interaction can be excluded in these materials due to the large distance between the Mn^{2+} ions which reduces the direct overlap between their wavefunctions (localization of spins). It is also possible (16) that in the case of zinc-blende structure, a screening effect of the direct interaction between the Mn^{2+} results from the presence of an anion atom partly between the two neighboring Mn^{2+} ions. Therefore an indirect exchange, which includes RKKY, mechanism should be considered. This type of mechanism may take different forms. As has been mentioned above, the RKKY interaction is not expected to have a significant contribution in some SMSC materials such as our alloy system. A second candidate is known as superexchange (19). This type of exchange is believed to be dominant in wide energy gap SMSC. The interaction between spins in this case is via a virtual transition between the valence band and the manganese ion energy levels. However, in narrow gap SMSC, a second type of mechanism is present in addition to superexchange. This mechanism describes the interaction as being channeled through the conduction band (Bloembergen-Rowland) model (24). A simple picture of these types of interaction is presented in figure (3.3). These models will be discussed in more detail in the analysis of the results.

3.3 EXPERIMENT

A SQUID (Superconducting Quantum Interference Device) magnetometer, figure (3.4), was used to measure the d.c. susceptibility in these semimagnetic semiconductors. This magnetometer consists of a double dewar cryostat of which the outer dewar is used as a helium reservoir and in which a Niobium superconducting solenoid is placed to supply a d.c. magnetic field. This solenoid is isolated from its surroundings by a lead shield in order to attenuate any

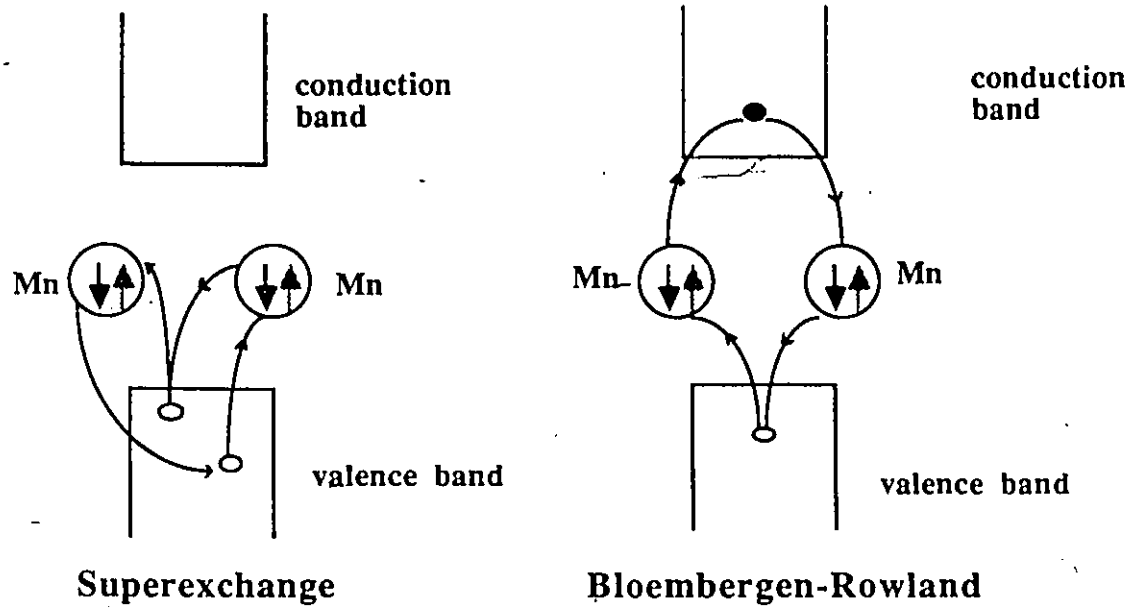

Figure 3.3 Different types of possible exchange mechanisms in SMSC materials.

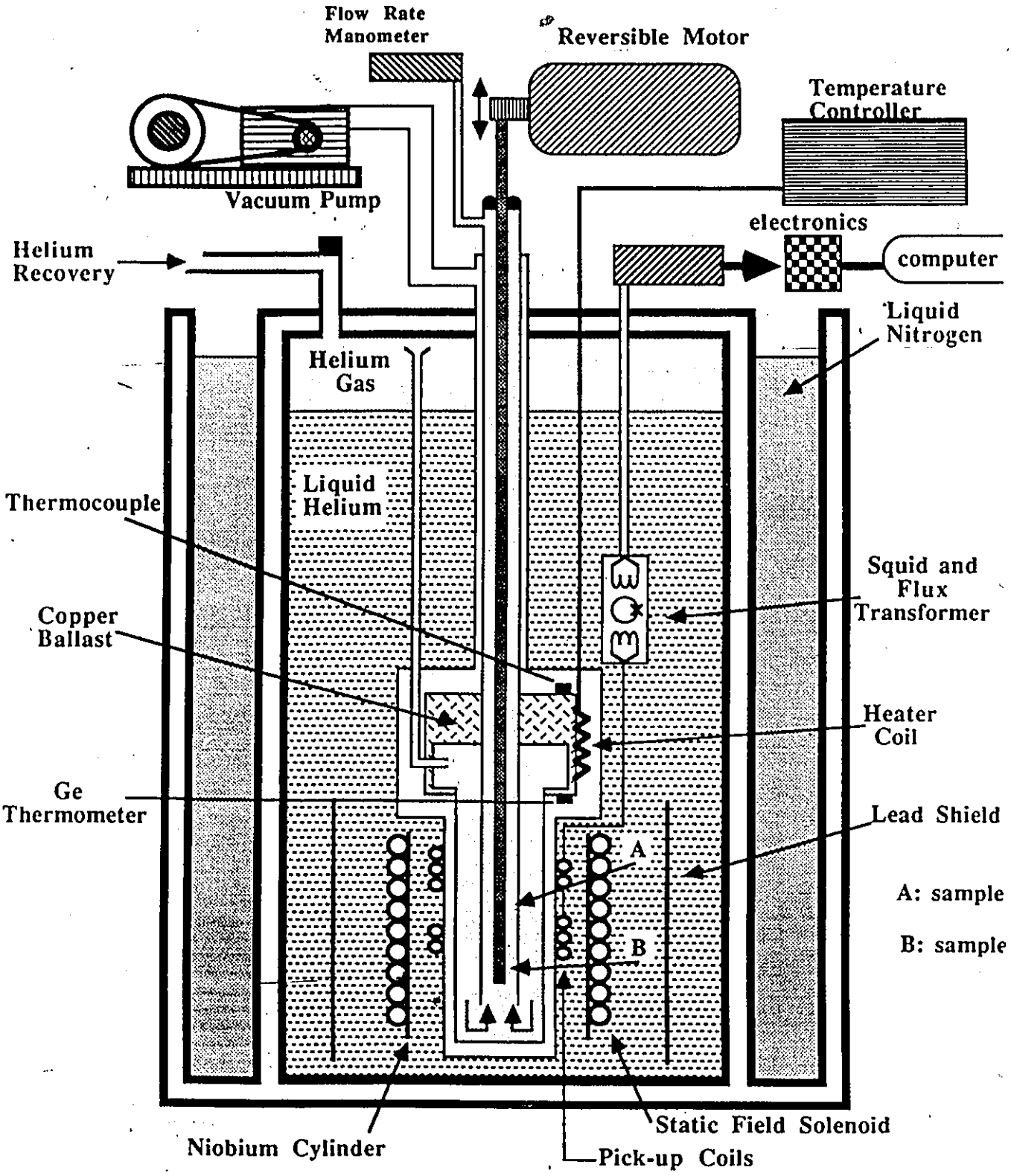

Figure 3.4 Magnetometer used in the measurements of d.c. magnetic susceptibility.

external magnetic noise. A Nb cylinder is used to trap a uniform magnetic field inside the area where the sample's magnetization is measured. Due to the very high sensitivity, ($2*10E^{-10}$ gauss cm^2) of the SQUID, only a small field is required (25 ~ 30 gauss) to induce the sample magnetization. Two superconducting pick-up coils are placed in the same reservoir inside the magnetic field. These two coils are wound in opposite directions, in order to allow cancellation of noise signals (as well as eliminating the current induced in them by the magnetic field). The inner dewar is isolated from the helium bath by a vacuum chamber. The temperature in this dewar can be controlled by regulating the temperature of the exchange gas flowing into the sample area. Measurements are performed on two samples at a time placed in a two compartments high purity copper holder. These two compartments are separated by approximately 4.5 cm from each other. The sample holder is attached to the end of a long plastic rod that extends to the outside of the cryostat, where it is connected to a motor driven displacement mechanism. The procedure followed in these measurements is first, to drive the sample holder upward allowing the first sample in the first compartment to pass through the two pick-up coils. Thus, two signals of opposite polarity, due to the opposite winding of the coils, are generated. The sum of these two signals is proportional to the magnetization of the sample. After the first sample passes out of the pick-up coils, the signal of the second sample is detected in the same sequence. This procedure is repeated for the two samples as the sample holder is driven downward and the signals are then averaged and stored by an APPLE mini-computer for further processing.

The range of temperature accessible by this magnetometer is between 4.2 K and room temperature; however, no measurements have been performed above 250 K, due to the excessive evaporation rate of helium in that range. The temperature of the samples was measured using a chromel : gold 0.07% iron thermocouple used in Air Product temperature controller (± 0.2 K over most of the temperature range). A calibrated germanium resistance thermometer was used in the low temperature range (4.2 K ~ 6 K) and served as a reference standard up to 100 K. The value of

the absolute magnetic susceptibility has been obtained by calibrating the apparatus with a small sphere of very pure lead that becomes a perfect diamagnet below 7.2 K. The susceptibility in absolute units (emu/gm) is then automatically obtained at the output of the magnetometer once the value of the magnetic field and the mass of the sample are known. The temperature accuracy in the range 10 ~ 100 K is ±.5 K and improves below that range. Between 100 ~ 250 K the accuracy decreases and is of the order of ±2 K.

Susceptibility measurements were usually carried out as follows. The samples were first cooled to the lowest obtainable temperature (4.2 K) outside the field (zero field cooling). Then the samples were lowered into the steady magnetic field (~25 gauss) in which the measurements of $\chi(T)$ vs T were taken up to a temperature well above the freezing point T_g. Then the samples were cooled back to 4.2 K in the field (field cooling) and the susceptibility of the sample was remeasured all the way up to 250 K. These two methods of cooling were performed in order to observe the "hysteresis" effect in $\chi(T)$ in these materials at temperatures below T_g, see below.

3.4 RESULTS

3.4.a Measurements of Freezing Temperature T_g

Magnetic susceptibility measurements were carried out on samples with Mn^{2+} concentration ranging up to 60%. Samples with zinc-blende crystal structure showed a single sharp cusp at some temperature T_g. This singularity in $\chi(T)$ is attributed to the random freezing of spins in the lattice as mentioned previously. When T_g is plotted versus the concentration of the manganese atoms (z), a straight line is obtained which extrapolates to $z \approx 0.2$. The intercept of this line, figure (3.5,b) agrees with the theoretical nearest neighbor percolation limit of 0.196 for fcc lattice structure (17,18). This percolation limit defines the concentration below which the system cannot sustain any freezing process that arises from nearest neighbor interaction. In such a case the

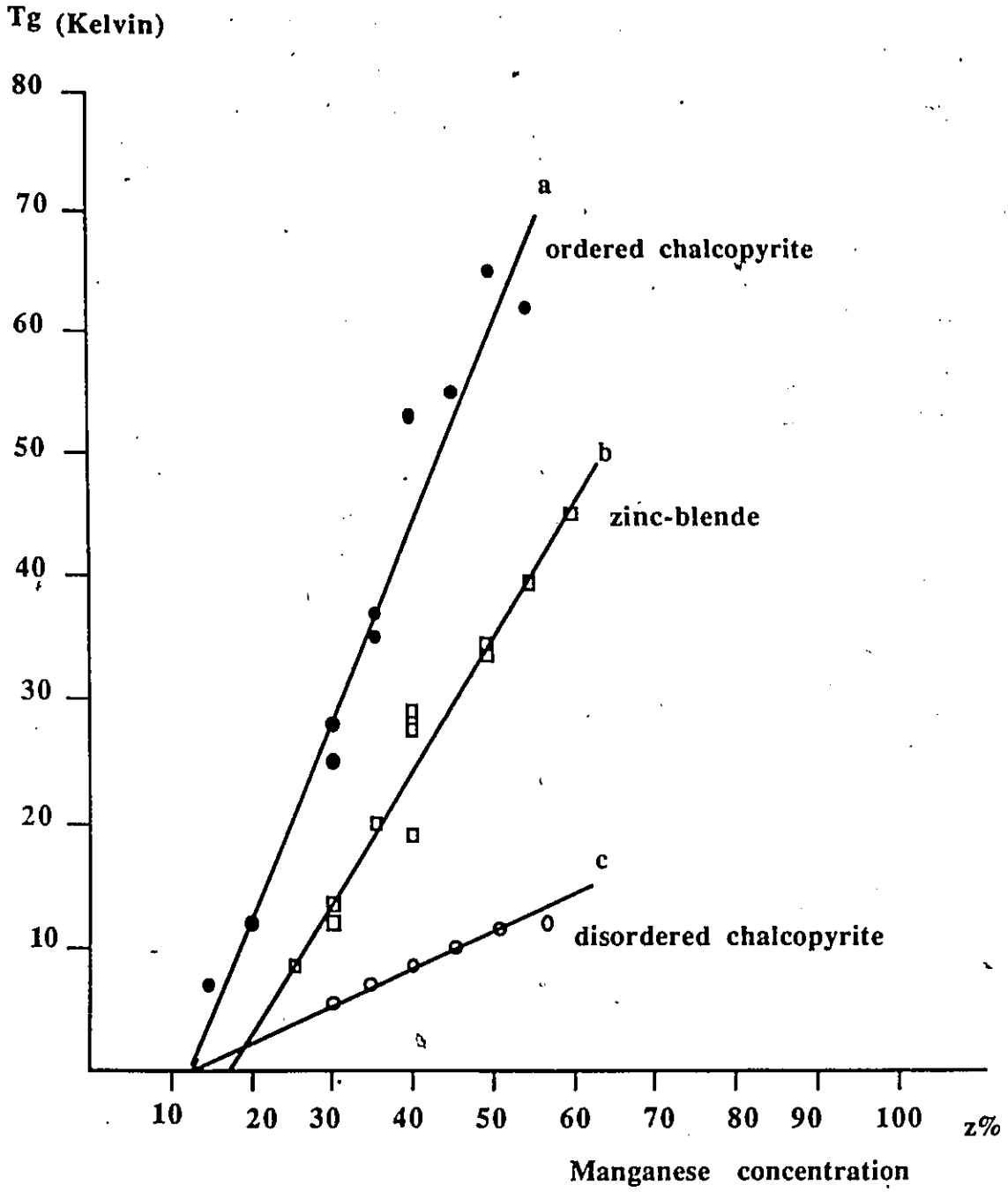

Figure 3.5 Variation of freezing temperature with manganese concentration.

material consists of small isolated non-interacting clusters. As a result of this, one would not expect the occurrence of any freezing at such Mn^{2+} concentration, and the material would be expected to remain paramagnetic down to 0 K. As the concentration is increased above that value, larger clusters are present, in such a way that they can overlap and therefore an infinite cluster forms eventually at T_g, leading to the freezing of the spins. Due to the limitation of the experimental set-up, no values of Tg that correspond to freezing arising from interaction between higher orders of nearest neighbors for concentration below z=0.20 could be observed in the case of zinc-blende samples, and z=0.15 for chalcopyrite samples, since these values are lower than 4.2 K. The scatter of the experimental values of T_g was found to be within the experimental error estimated from the accuracy in weighing the sample components, non-stoichiometric effects, etc.

Some chalcopyrite samples showed two maxima in their χ vs. T relation, see figure (3.6). In this figure a maximum is observed at T_g which corresponds to the spin glass freezing and another maximum is observed at T_N that corresponds to the antiferromagnetic ordering of the spins experienced by some parts of the sample. The observation of these two maxima suggests the presence of two magnetic phases in the material. These two phases, however, could not be identified in the x-ray analysis. As discussed earlier, it is difficult to obtain samples that show solely one of these types of magnetic behaviors, due to the fact that the material may not be quenched rapidly enough. The rate of cooling of the sample from the annealing temperature (650 ^{o}C) was found to affect the relative magnitudes of the two maxima. Most of the samples presented in figure (3.5,a,c) have been cooled slowly in the furnace by turning it off at 650 ^{o}C and letting the samples reach room temperature over several hours. Thus, in these cases one expects the samples to be mostly ordered since the material spends long enough time in the ordering region, and that is identified by the strong peak at T_N. However a faint second maximum is present due to some disordered regions in the sample.

As mentioned before, the magnetic susceptibility of all samples have been measured

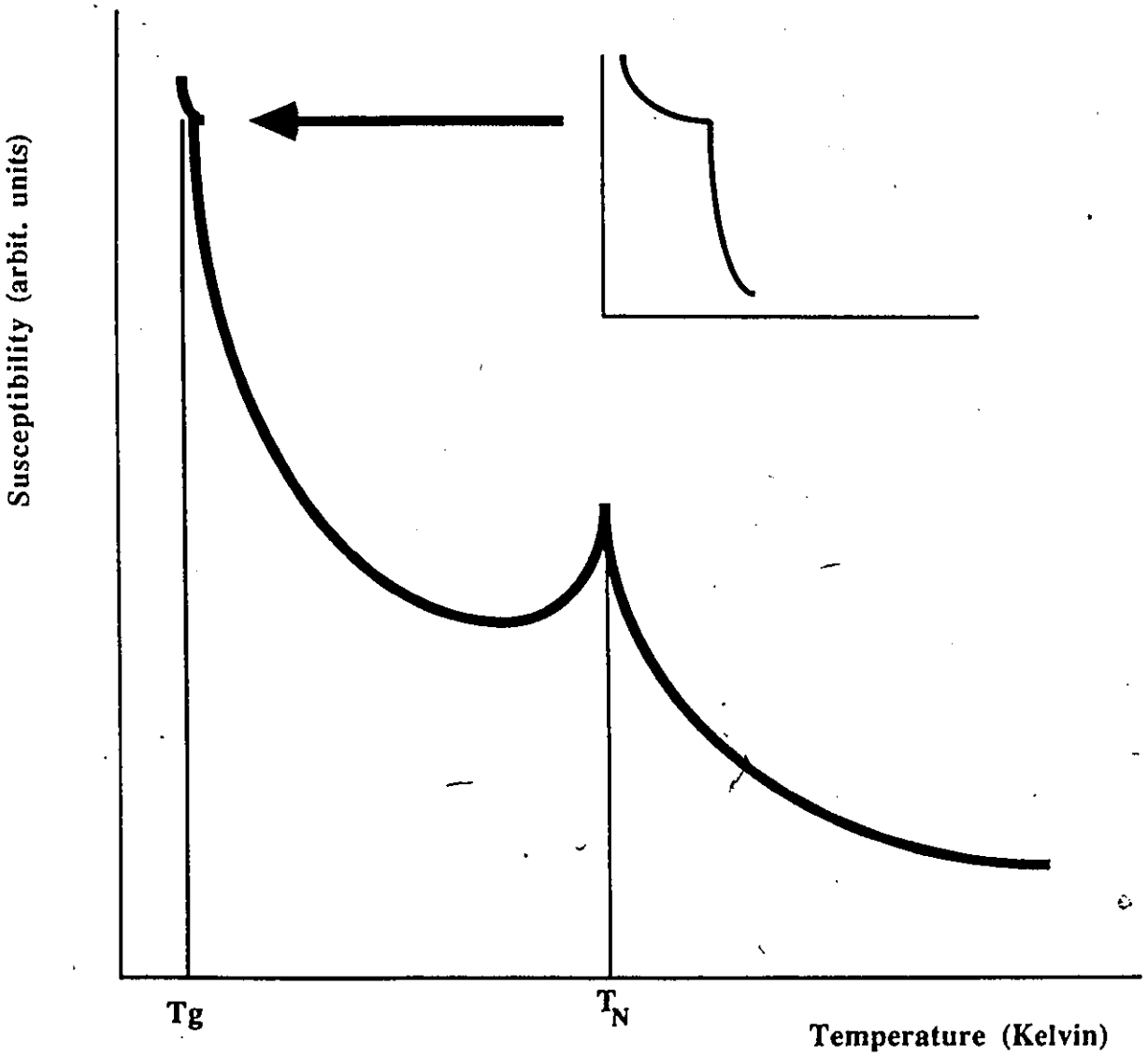

Figure 3.6 Typical behavior of chalcopyrite sample in the susceptibility versus temperature variation showing two maxima at Tg and T_N.

under zero field cooling (ZFC) condition as well as under field cooling (FC). The susceptibility measured under these two conditions are different for temperatures below T_g, figure (3.7). This difference is regarded as an irreversible effect due to the fact that some of the spins will retain their alignment after being cooled in the field. This procedure was often helpful in the determination of T_g in the cases where the susceptibility cusp are not pronounced. In chalcopyrite samples this irreversible effect is observed only for $T<T_N$ and not at T_g, figure (3.8).

3.4.b DETERMINATION OF CURIE-WEISS TEMPERATURE

Plotting the inverse of the susceptibility versus temperature results in a straight line in the high temperature region, indicating that the sample behaves paramagnetically and in accordance with Curie-Weiss law (28):

$$\chi = \frac{c}{T-\theta}$$

$$\frac{1}{\chi} = \frac{T}{C} - \frac{\theta}{C}$$

When extrapolated back to $1/\chi = 0$, the intercept of this line on the T axis, figure (3.9), gives the value of the Curie-Weiss temperature θ. The slope of this line on the other hand provides the value of the Curie constant C in (K.emu/mol). In figure (3.10) values of θ are plotted vs. "z", (the Mn^{2+} ion concentration) for some chalcopyrite and zinc-blende samples. Due to the mixture of the ordered and the disordered phases in the chalcopyrite samples, θ in this case represents only a weighted average of the contributions of the two phases. Thus no distinction between the two phases could be inferred from this graph. Values of θ were negative for all our samples over all ranges of solid solution. This indicates that the antiferromagnetic type of coupling of the spins is

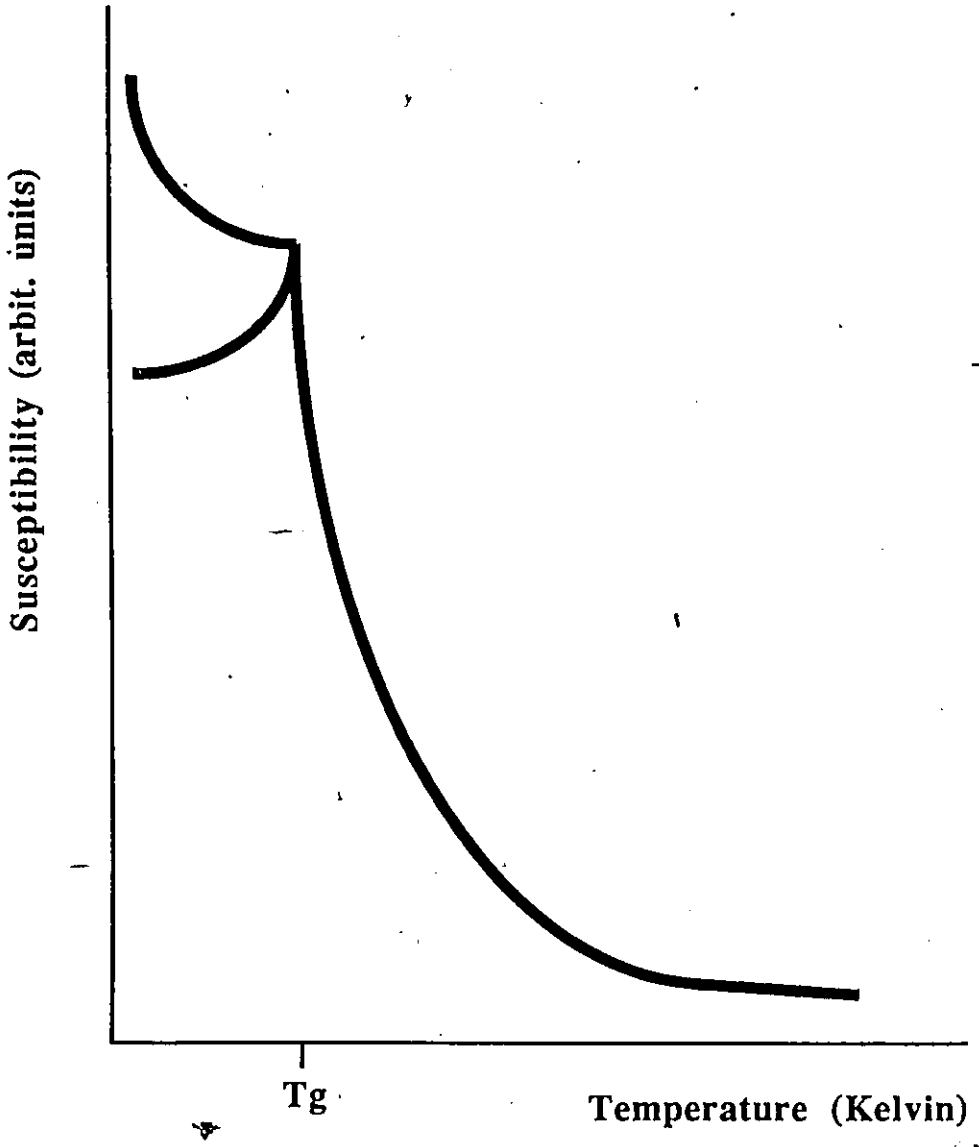

Figure 3.7 Irreversible effect in magnetic susceptibility above Tg.

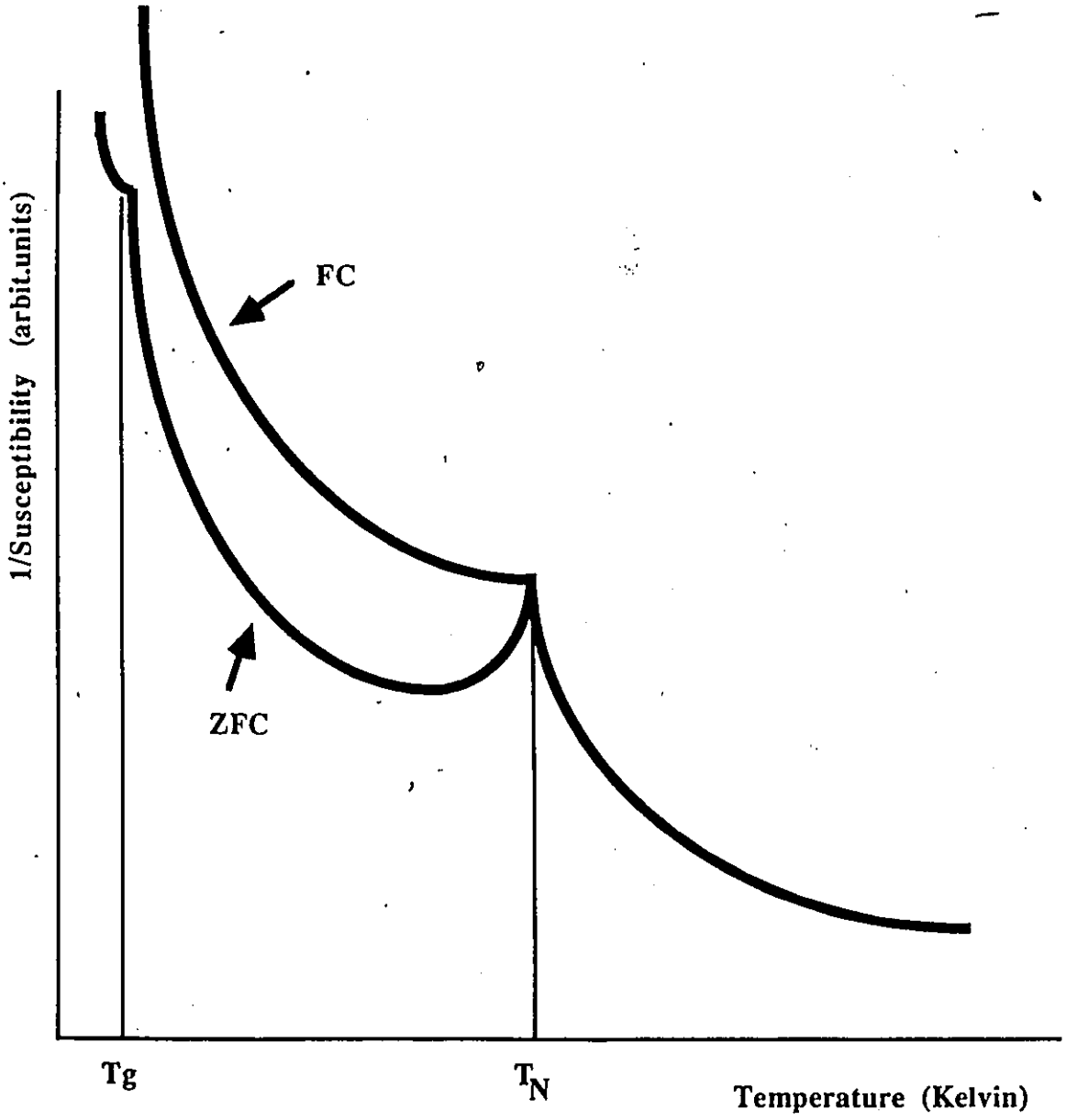

Figure 3.8 Irreversible effect in magnetic susceptibility in a chalcopyrite sample having two maxima.

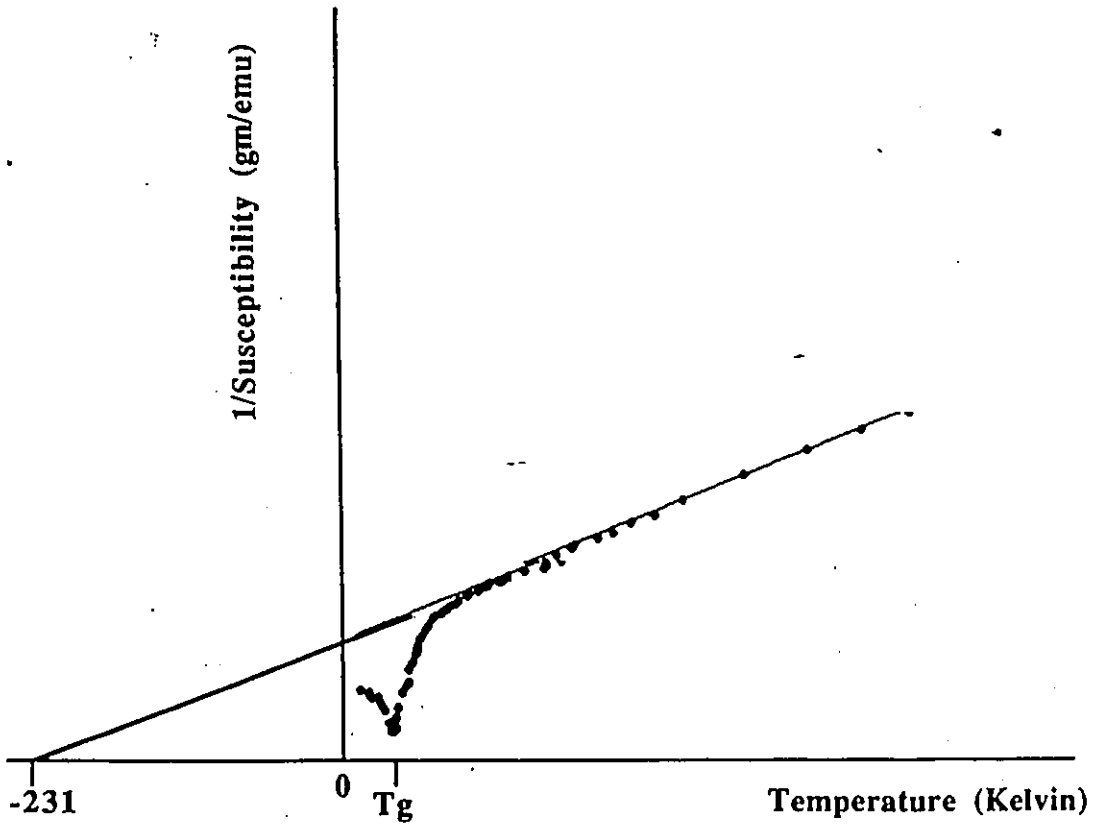

Figure 3.9 Inverse of magnetic susceptibility versus temperature for zinc-blende sample with x=.35, y=.35, z=.30.

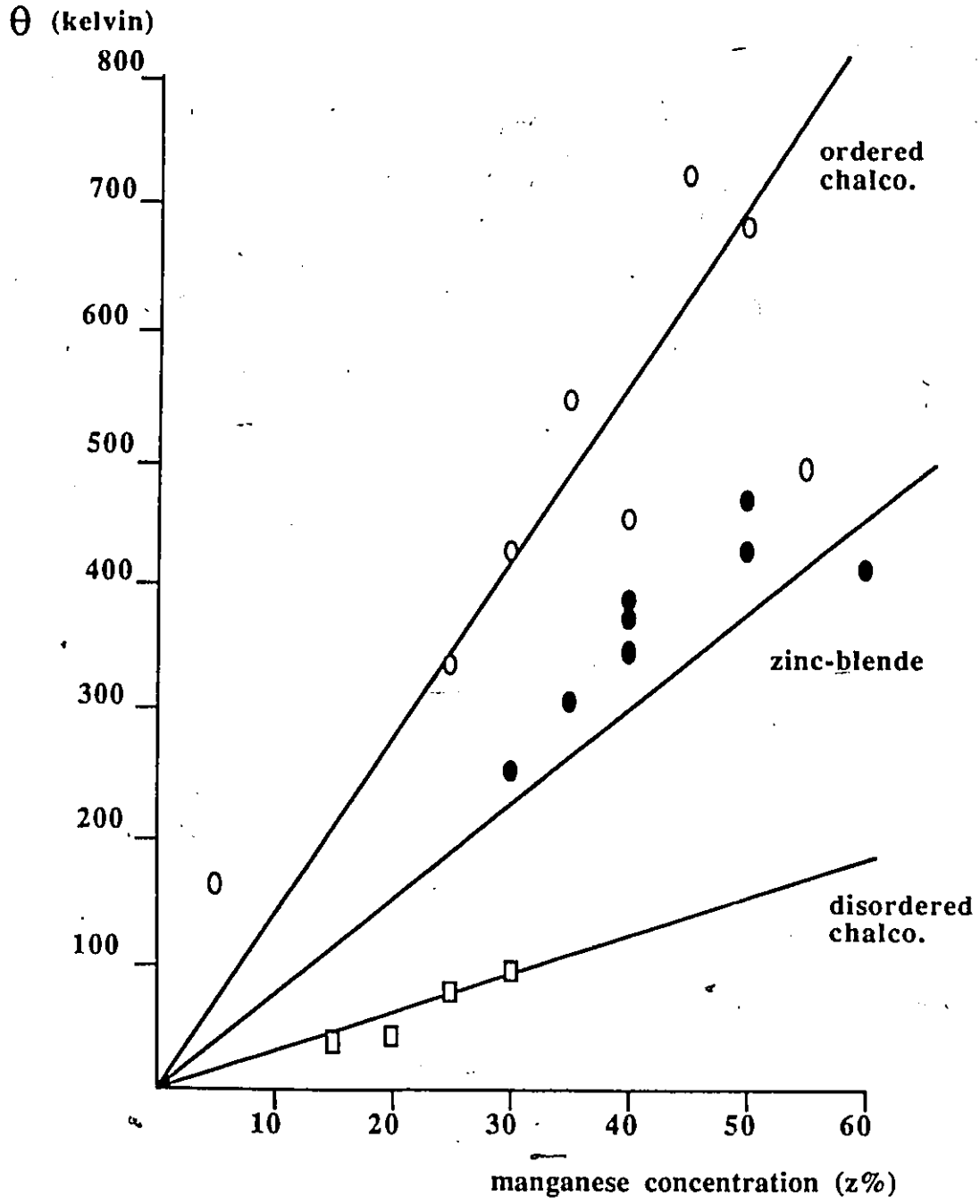

Figure 3.10 Variation of Curie-Weiss temperature with manganese concentration. Solid lines represent calculated values. Values for disordered chalcopyrite are obtained from ESR measurements.

dominant in these materials. In all samples, a clear deviation from the straight line representing the paramagnetic behavior could be observed at temperatures above T_g. This deviation is due in part to the enhancement of the paramagnetic phase by the formation of superparamagnetic clusters discussed earlier in this chapter.

3.5 ANALYSIS

In order to have an understanding of the freezing phenomenon in these spin glass materials as well as the magnetic behavior of the ordered phase, one should have a clear picture of the nature of the exchange interaction involved. In the actual fitting of the experimental data to any model, one encounters a difficulty arising from the simultaneous contribution of more than one magnetic behavior to the results. Therefore, and as will be seen later, we observed that the experimental values of θ lie between the two theoretically predicted values for the two phases involved. It is important, however, to mention that in the case of a few samples, the values of θ were found to confirm the calculated value for either one phase or the other, depending on the degree of order and disorder existing in the sample. It is also important to bear in mind, that it is possible that some parts of the chalcopyrite samples of concentration above ~0.4, are of zinc-blende structure. This mixture of the two structures becomes evident by considering the present phase diagram (temperature versus composition) to be similar to that of $(CuIn)_{1-z}Mn_{2z}Te_2$ (27), in which the material has the possibility of crystallizing in either one of the lattice structures, see figure (3.11). Although one expects a similar kind of phase diagram in our alloy system, the exact position of the boundaries separating the phases could be different. The presence of such a mixture could not be identified in the x-ray analysis of these materials due to the fact that the lattice parameters for both structures are almost equal. However, the effect of this mixture on the experimental values of θ could be clearly observed, where some of the samples with $z > 0.4$ tend to lie between the line of the zinc-blende and that of chalcopyrite. The effect of this mixture was also

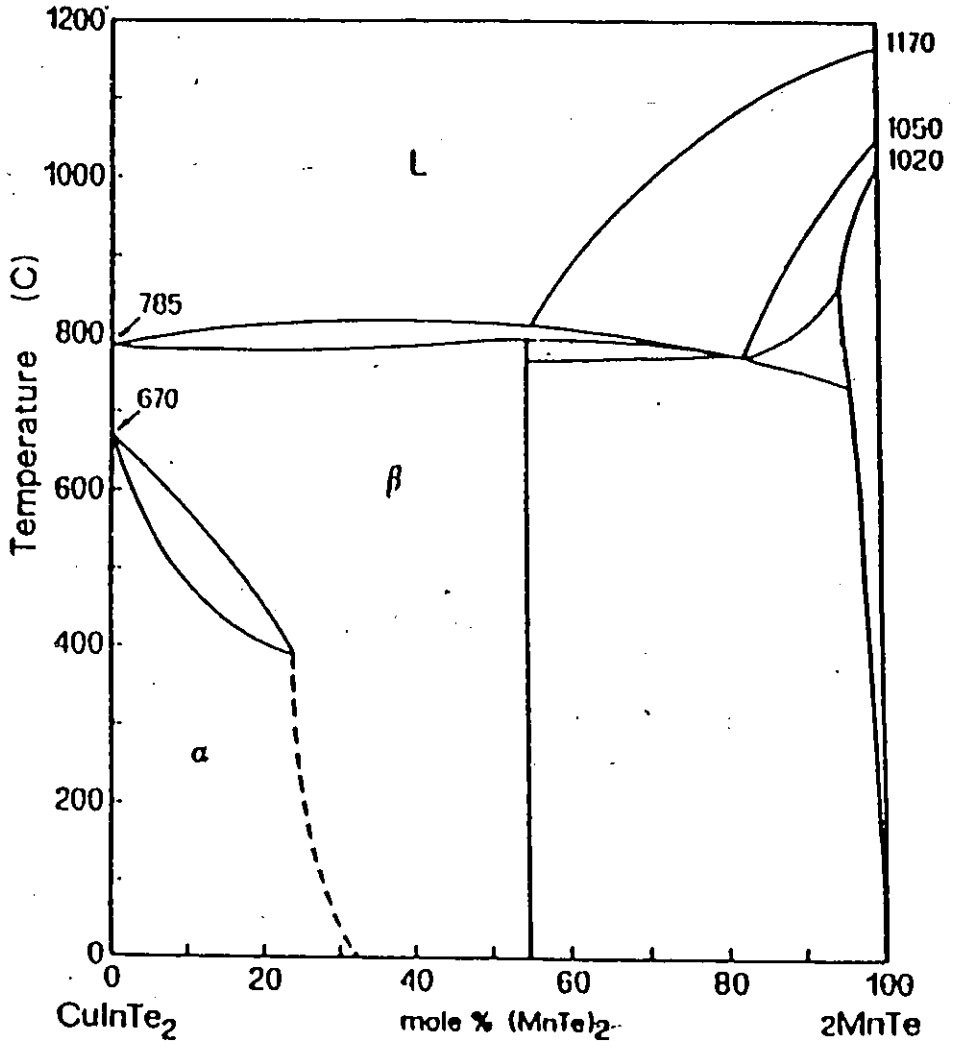

α = zinc-blende β = chalcopyrite

Figure 3.11 Proposed phase diagram for the system $CuInTe_2$ -MnTe. See reference (27) for details.

observed in the results of the ESR measurements that will be discussed in the following chapter.

According to the model proposed by Escorne et. al (20,15) there is an exponential variation of the exchange parameter "J" with the distance between the manganese ions, that is given by the following expression

$$J = J_0 \, e^{-\alpha r} \qquad (3.2)$$

where α and J_0 are constants, and "r" represents the distance between the Mn^{2+} ions. For SMSC with concentration "z" of manganese ions arranged randomly on a face centered cubic lattice, the nearest neighbor-spacing between the Mn^{2+} ions is given by

$$d = \frac{a}{\sqrt{2}}$$

and hence the mean spacing between the magnetic ions is $(dz^{-1/3})$. Therefore, the mean exchange interaction between the ions is

$$J = J_o \, e^{-\alpha d z^{-\frac{1}{3}}} \qquad (3.3)$$

As in the development of the theoretical model for antiferromagnetic materials, one expects the spin glass freezing to occur when the thermal energy becomes equal to the exchange energy at the freezing temperature T_g, i.e.

$$k_B T_g = -A \, J_o \, e^{-\alpha d z^{-\frac{1}{3}}} \qquad (3.4)$$

where k_B is the Boltzmann factor and "A" is a constant independent of "z". It is convenient to rewrite equation (3.4), by taking the logarithm of both sides and rearranging the terms to obtain the following expression

$$\ln T_g = \ln\left(-\frac{A J_o}{k_B}\right) - \alpha d z^{-\frac{1}{3}} \qquad (3.5)$$

Therefore, a plot of the experimental values of ($\ln T_g$) versus $dz^{-1/3}$ is expected to give a straight line if equation (3.2) holds.

Such a plot is presented in figure (3.12). It is seen that the experimental points fall on three different straight lines representing the zinc-blende and the ordered and disordered chalcopyrite samples. It should be noted that the mean spacing between the Mn^{2+} ions in the case of the chalcopyrite lattice is very similar to that of zinc-blende, since the ratio c/a is very close to 2, and therefore, has a small effect on the mean spacing "d".

From these plots and equation (3.5), it is clear that "α" is a constant independent of the manganese concentration, as well as of the ratio of y to x, and therefore, independent of various parameters that vary with concentration, such as the energy gap. This type of analysis was performed on other SMSC, $Cd_xZn_yMn_zTe$ for example (25), and a similar behavior of the constant "α" was observed.

Equation (3.2) represents an empirical relation that does not give any physical insight as to the mechanism of exchange involved in these materials. One of the models that gives such insight is the Bloembergen-Rowland (24). In this model the interaction between the ions takes place via virtual transitions between the valence band and the conduction band. The variation of the

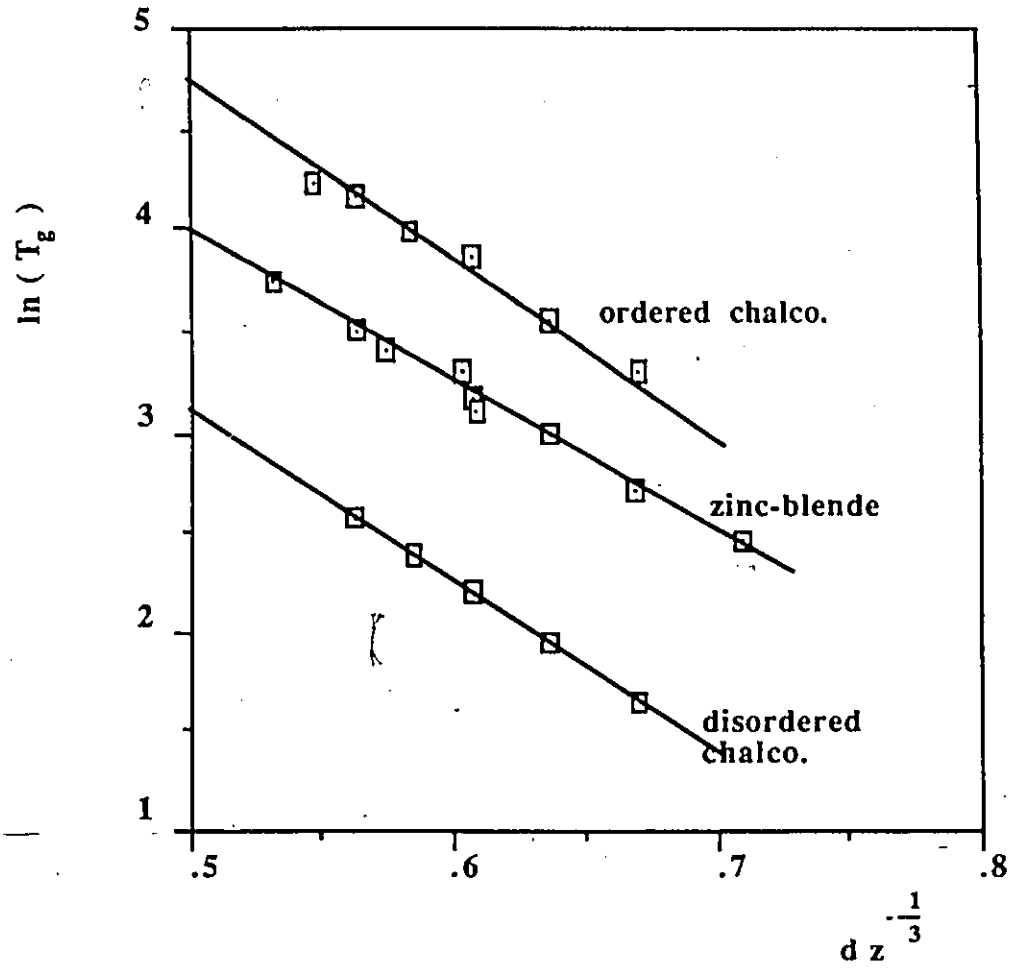

Figure 3.12 Fitting of experimental data to equation (3.5).

exchange parameter with distance between the ions also has an exponential form in this model, with the exponent being a function of the energy gap E_g. This model is expected to be of importance in low band gap materials such as $Hg_{1-x}\,Mn_xTe$ where there is a high probability of a virtual transition across the gap (3,5,26). On the other hand this type of mechanism is not expected to be dominant in our material where the energy gap values are considerably higher. For instance, according to reference (19), the contribution of such mechanism is estimated to be of the order of 5% in the case of $Cd_{1-x}Mn_xTe$ in which the energy gap varies from 1.5 to 2.5 ev over the entire range of composition. Therefore one may expect a contribution of such percentage or slightly higher in our alloys. According to this model, the variation between the exchange parameter and the ionic spacing can be written as follows

$$J(R_{ij}) = \frac{C}{R_{ij}^3}\, e^{-\alpha R_{ij}} \qquad (3.6)$$

where

R_{ij} = distance between the i^{th} and j^{th} spins

$\alpha = [\,2 m_c E_g / h^2\,]^{1/2}$

C a constant

m_c conduction band effective mass

E_g energy gap

Due to the difficulties in the determination of E_g over the entire range of solid solution, which will be discussed in the next chapter, the exact contribution of such mechanism could not be determined. In order to obtain the results of energy gap measurements over all the range of solid

solution, a different method of the sample heat treatment is probably required, especially in the case of chalcopyrite samples. Because of the time limitation and the effort involved, this task became beyond the scope of this report, and therefore, no conclusion could be drawn in this regard. However, since this contribution is expected to be of the order of 5% only, it can be neglected anyway.

Another model for the exchange mechanism in SMSC is that proposed by Geertsma et. al (21), which is based on the work of Gonçalves da Silva and Falicov. In this model the interaction between the magnetic ions takes place via a virtual transition between the valence band and the delocalized $3d^5$ state of the manganese ion. The variation of the exchange parameter is then written as

$$J(R_{ij}) = J_o R_{ij}^2 \, e^{-\alpha R_{ij}} \qquad (3.7)$$

and by following the same argument used above in equation (3.5), this expression can be written as

$$\ln(d^2 T_g z^{-\frac{2}{3}}) = \ln\left(\frac{-A J_o}{k_B}\right) - \alpha d z^{-\frac{1}{3}} \qquad (3.8)$$

The exponent "α" in equation (3.7) is a function of the energy of interaction and the effective mass of the valence band (22)

$$\alpha = \varepsilon \left(\frac{2 m^*}{h^2}\right)$$

where ε represents the energy difference between the $3d^5$ and the excited $3d^6$ levels of the Mn^{2+} ion.

Our experimental results are replotted in terms of $(\ln d^2 T_g z^{-2/3})$ versus $(dz^{-1/3})$ as in figure (3.13). Again the experimental values were found to give straight lines, within experimental error, for the three different phases that exist in the material. The values of α and (AJ_o/k_B) for the three different phases were then determined from the slopes and the intercepts of these lines.

The next step is to use the values of α and (AJ_o/k_B) determined above to predict the Curie-Weiss temperature θ. This could be accomplished by using the mean field theory of antiferromagnetic materials (23), given by

$$\theta = \frac{2}{3}\frac{s(s+1)}{k_B}\sum_i n_i J_i \qquad (3.9)$$

where

J_i is the exchange parameter for Mn^{2+} i^{th} nearest neighbors

n_i is the number of the i^{th} nearest neighbors

Thus θ is the sum of the contributions of all consecutive sets of neighbors given by the index (i). If J_i is replaced by the expression in (3.5), then (3.9) becomes

$$\theta = \frac{2}{3}\frac{s(s+1)}{k_B} z J_o \sum_i \frac{n_i e^{-\alpha d_i}}{d_i^2} \qquad (3.10)$$

where d_i is calculated up to the 6^{th} nearest neighbor spacing. Contributions of the 7^{th},

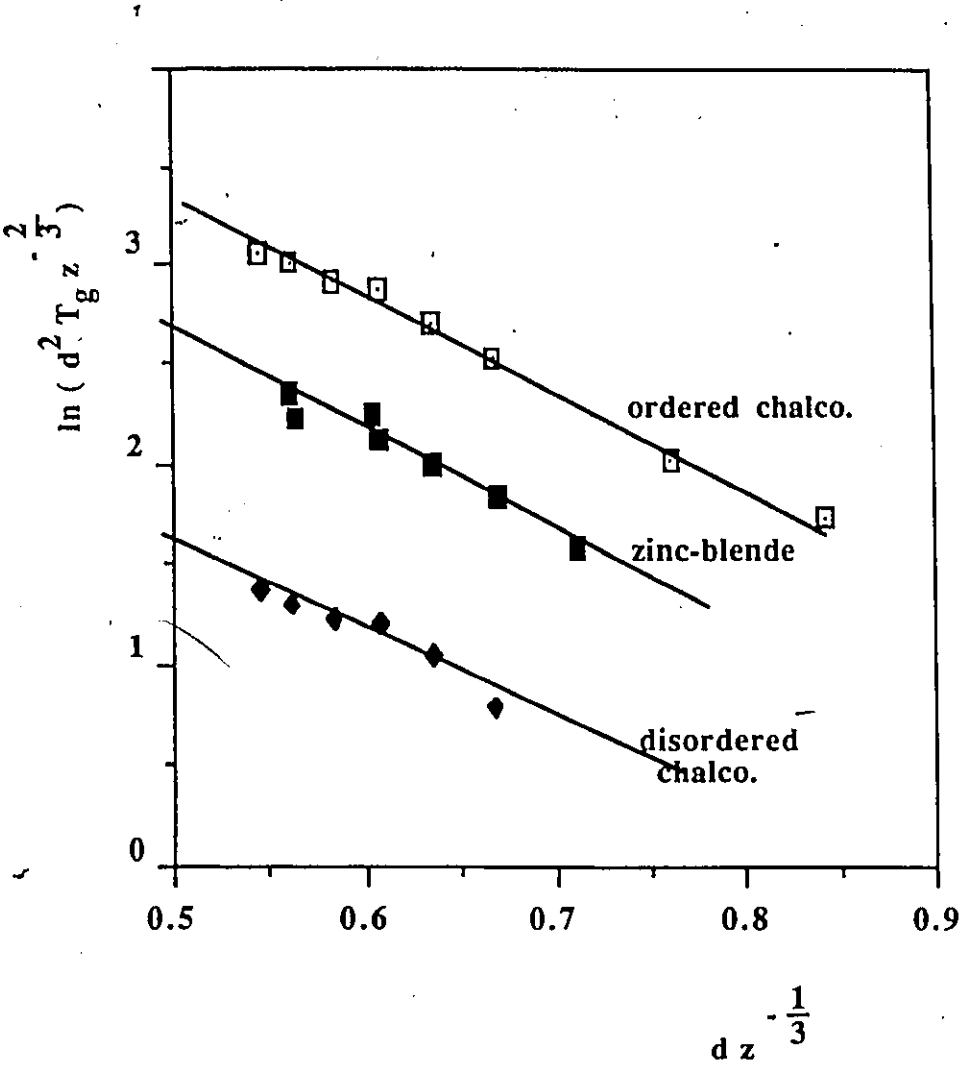

Figure 3.13 Fitting of experimental data to equation (3.8). The values of the slopes and intercepts are given in tables 3.1,3.2 and 3.3.

8^{th} etc. nearest neighbors were found to be negligible.

The values of "α", ln ($d^2 T_g z^{-2/3}$), "a", "T_g", as well as the experimental and calculated values of θ are given in tables (3.1), (3.2) and (3.3) for zinc-blende, ordered and disordered chalcopyrite samples respectively.

Unfortunately, it has not been possible to obtain completely ordered or completely disordered chalcopyrite samples due to difficulties discussed in chapter 1, and therefore, the two lines for θ vs. z calculated for the ordered and disordered phases, see figure (3.11), give only upper and lower limits with respect to the experimental data. This is due to the fact that the measured value of θ represents the weighted average of the contributions of the two phases. It can be clearly seen that experimental values of θ in the case of chalcopyrite samples fall closer to the line calculated for the ordered structure than to the line calculated for the disordered structure, figure (3.10). This indicates then, that these samples are mostly ordered. This is confirmed by the measurements of magnetic susceptibility, where the intensity of the maximum at T_N is significantly higher than that at T_g. Experimental values of θ for the disordered chalcopyrite samples could not be obtained from the magnetic susceptibility measurements, owing to the fact that such values were masked by the presence of the ordered structure. However, the analysis of the ESR results provided these values, figure (3.10), which is the subject of the next chapter.

As mentioned before, no information about the exact type of ordering of the Mn^{2+} ions could be obtained from the x-ray analysis, and neutron diffraction measurements are now being carried out by another member of the research group on this alloy system for that purpose. However, the calculated values of θ were based on two postulated possible types of ordering. In these two postulates we assumed that the manganese ions will reside solely on either one of the sublattices of the structure. The calculation of the Curie-Weiss temperature using either one of these postulates gave the same value of θ, with a difference comparable to the experimental error. This insensitivity of the measurement to the type of ordering could be understood by

considering the fact that the mean distance between nearest neighbors as well as the number of nearest neighbors would not change.

composition	T_c(K)	a_o(nm)	θ_{exp}(K)	θ_{cal}(K)
17.5/52.5/30	15	.6335	-254	- 233.7
15/50/35	20	.6332	-317	- 273.1
30/30/40	27	.6287	-387.4	321.1
15/45/40	20	.6337	-350.8	- 311.2
10/50/40	24	.6329	-321.7	- 312.7
25/25/50	33	.6318	- 428	- 393.7
2.5/47.5/50	30	.6438	-478.8	-365.1
20/20/60	35	.6339	-403	-466.2

α= -4.489

Ln (- A J_o / k_B) = 4.8515

d_i		$a/\sqrt{2}$	a	$\sqrt{3/2}\,a$	$\sqrt{2}\,a$	$\sqrt{10/2}\,a$	$\sqrt{3}\,a$
n_i	—	12	6	24	12	24	8

Table 3.1 Experimental and calculated data for zinc-blende samples.

composition	T_c(k)	a_o	θ_{exp}(k)	θ_{cal}(k)
00/95/05	--	.6309	-168	-67.3
00/75/25	11.5	.6322	-334	-333.6
00/70/30	27	.6341	-433	-395.5
00/65/35	35	.6335	-557	-463
00/60/40	60	.6329	-450	-531.4
00/55/45	54	.633	-734	-597.4
00/50/50	64	.6323	-684	-666.3
00/45/55	61	.6335	-496	-727.8

$\alpha = -4.6357$

$\mathrm{Ln}\,(- A J_o / k_B) = 4.8515$

d_i	$a/\sqrt{2}$	a	$\sqrt{3/2}\,a$	$\sqrt{2}\,a$	$\sqrt{10/2}\,a$	$\sqrt{3}\,a$
n_i	8	8	32	8	12	0

Table 3.2 Experimental and calculated data for ordered chalcopyrite samples.

composition	T_c(k)	a_o	θ_{exp}(k)	θ_{cal}(k)
00/95/05	--	.6309	---	-15.1
00/85/15	--	.6321	-40	-50
00/80/20	--	.6301	-42	-65
00/75/25	--	.6322	-75	-75.2
00/70/30	6	.6341	-95	-89.5
00/65/35	7	.6335	---	-104.6
00/60/40	9	.6329	---	-119.9
00/55/45	10	.633	---	-134.8
00/50/50	11.6	.6323	---	-150.3
00/45/55	12	.6335	---	-164.4

$\alpha = -2.6935$

$\text{Ln} (- A J_o / k_B) = 2.788$

d_i	$a/\sqrt{2}$	a	$\sqrt{3/2}\,a$	$\sqrt{2}\,a$	$\sqrt{10/2}\,a$	$\sqrt{3}\,a$
n_i	12	6	24	12	24	0

Table 3.3 Experimental and calculated data for disordered chalcopyrite samples.

CHAPTER 4
ELECTRON SPIN RESONANCE MEASUREMENTS

4.1 INTRODUCTION

The application of a static magnetic field "H" to a free magnetic ion possessing a permanent magnetic moment results in the Zeeman splitting of its energy levels as given by

$$E = M_S \, g \, \mu_B \, H \qquad (4.1)$$

Where

M_S is the spin magnetic quantum number

g is the Landé splitting factor

μ_B Bohr magneton

In Electron Spin Resonance (ESR), transitions between these levels, which obey the selection rule $\Delta M_S = \pm 1$, are induced by the application of an alternating electromagnetic field with an angular frequency (28) w, given by

$$\hbar w = g \, \mu_B \, H \qquad (4.2)$$

corresponding to the energy difference between the adjacent magnetic energy levels and separated by $\hbar w$.

In our alloy system $Cd_{2x}(AgGa)_y \, Mn_{2z}Te_2$, the Mn^{2+} ions possess a permanent magnetic moment with a spin S=5/2 corresponding to a $3d^5$ atomic configuration. The application of a magnetic field will split the energy levels as shown schematically in figure (4.1 a). Due to the effect of a cubic or nearly cubic crystalline electric field, further splitting of the energy levels

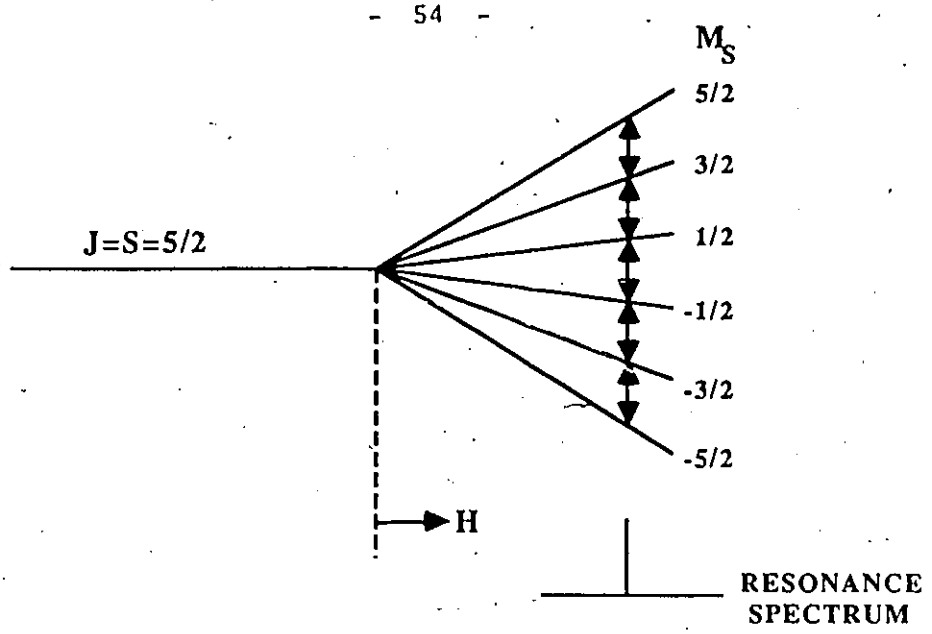

Figure 4.1 a. Free ion Zeeman Splitting of a $3d^5(^6S_{5/2})$ level. In this example there is only one resonance line.

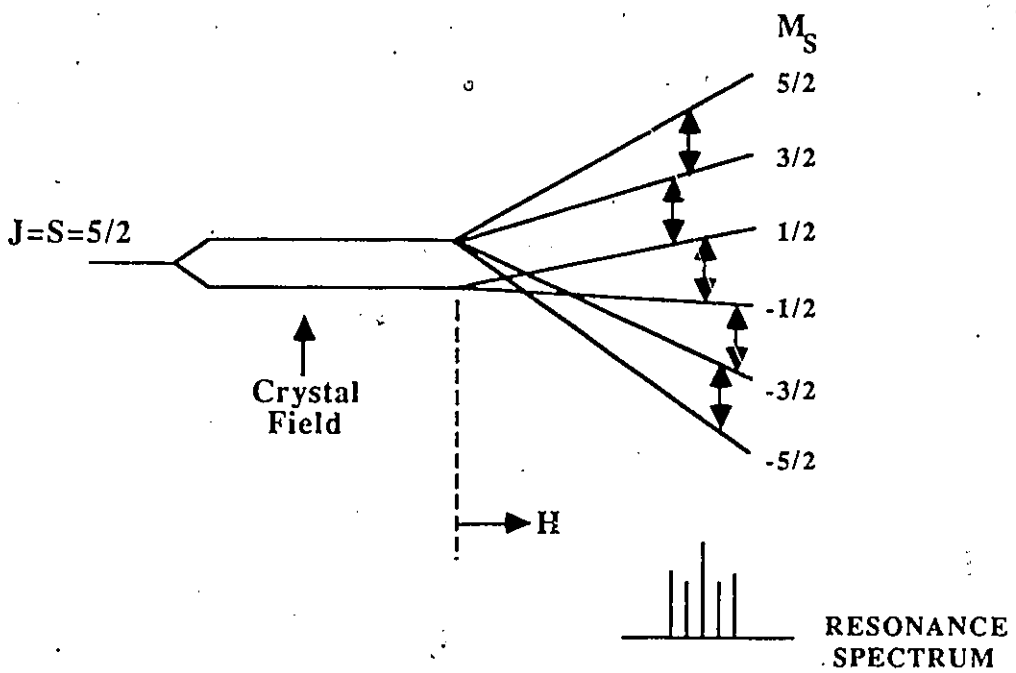

Figure 4.1 b Zeeman Splitting of a $3d^5$ ($^6S_{5/2}$) level with Fine structure Splitting. The single resonance line is split into five by the presence of a crystal field.

results, figure (4.1 b).

In usual ESR measurements, the transition between these energy levels is induced by fixing the frequency of the incident radiation, at some point in the microwave range, while varying the magnetic field. For systems of free ions in thermal equilibrium, the population will be largest for the low energy levels. Therefore, in spite of the equal probability of absorption or emission, a net amount of the incident radiation will be absorbed by the material that can be detected experimentally. This effect is manifested as a broad maximum in the absorption spectra of these materials. The reason for having such maximum that is spread over a wide range of H, instead of a well defined value, is the presence of dipole-dipole interaction, exchange interaction and various types of relaxation phenomena, such as spin-spin and spin-lattice (28).

Electron Spin Resonance measurement was found to be a very effective experimental method of studying this type of magnetic systems. The observations provided by this method reveal information concerning the exchange interaction between the spins. Also, performing this type of study on these materials provides valuable information about the dynamics of the magnetic system as well as the critical phenomena that occur when the temperature is varied. One other importance of such measurements is that it has been employed as a method of detecting the existence of order and disorder in our samples, as well as the degree of such order. This is discussed in the following sections of this chapter.

These measurements were performed in the ESR laboratory at the University of Ottawa by the technician specialist Mr. Bei Wah Chan, under the supervision of Professor A. Manoogian.

4.2 MEASUREMENTS

Most of the samples that have a single crystallographic structure were studied by this technique. The range of temperature over which the experiment was performed was between 550 ~

90 K in two steps: from room temperature down to 90 K, and from room temperature up to 550 K. No measurements in the low temperature range of (90 to 4.2 K) could be performed due to some damage to the helium-transfer equipment in our laboratory. There was only one exception to this: a sample with composition (x=0, y=0.75, z=0.25), a chalcopyrite, has been studied in the range of 90 ~ 4.2 K. This set of measurements was performed at the National Research Council laboratories by Dr. Bartkowski whose help is gratefully acknowledged.

A detailed description of the experimental set-up used in these measurements as well as of the procedure followed is given by Chehab (29). The apparatus consists mainly of an electromagnet, a microwave source (~9.4 GHz) and a system of waveguides that direct the microwave energy to the sample. In order to simplify the determination of the linewidth in these measurements, the derivative of the absorption signal is taken by applying a modulating signal to the static magnetic field. This modulation (100 kHz) is realized by means of two Helmholtz coils mounted on the two opposite walls of the sample's cavity facing the two poles of the electromagnet. The linewidth ΔH was taken as the peak to peak separation of the derivative curve, as illustrated in figure (4.2). In figure (4.2 a), the modulation field causes the microwave power in the cavity to be modulated at the same frequency when the sample absorbs power at resonance. As the steady field is slowly swept through the absorption curve, the amplitude of the modulation of the microwave power changes in proportion to the absorption curve as shown in figure (4.2 b). The modulated microwave power travels from the cavity to the crystal detector where it is demodulated and then passes to a phase sensitive detector. The output of the phase sensitive detector gives the first derivative pattern of the ESR line on a chart recorder as shown in figure (4.2 c).

The temperature of the sample was controlled within ± 2 K over the entire range indicated above, by circulating nitrogen gas evaporated from liquid for measurements in the low temperature region, and by a flow of properly heated nitrogen gas in the high temperature region, around the

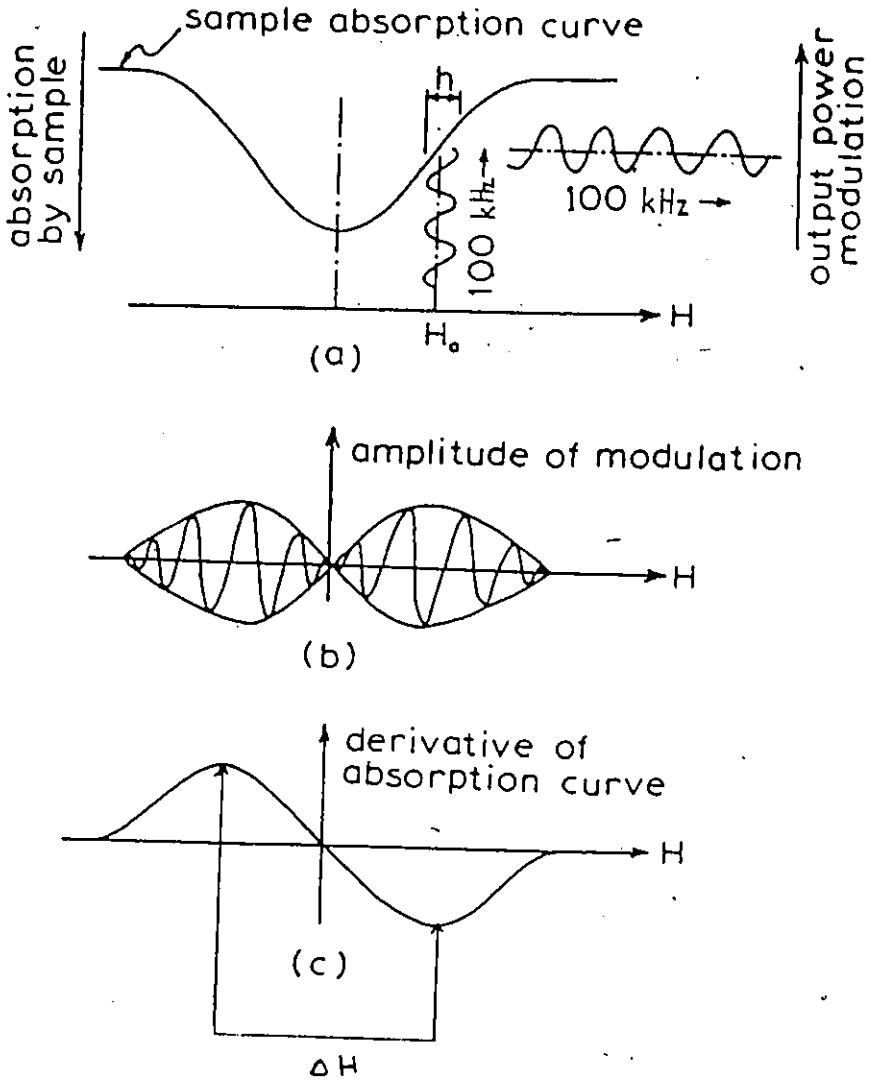
sample absorption curve
absorption by sample
h
100 kHz
100 kHz
output power modulation
H
H_o
(a)
amplitude of modulation
H
(b)
derivative of absorption curve
H
(c)
ΔH

Figure 4.2

sample. The temperature was measured with a thermocouple which was in direct contact with the sample. A gold-chromel thermocouple was used for temperatures below room temperature, and a copper-constantan thermocouple was used for temperatures above that. The procedure followed in these experiments is as follows: the sample was-placed in a glass tube mounted inside the microwave cavity and its temperature was stabilized at a certain value, and then the magnetic field was slowly swept over a range of 5 K gauss. The temperature was then changed (by controlling the temperature of the circulating nitrogen gas) by 50 K increments for temperatures above room and by 15 K for temperatures below that. The incident electromagnetic radiation will be absorbed by the sample when the resonance condition given by equation (4.2) is satisfied. This absorption was detected as a reduction in the intensity of the microwave radiation leaving the cavity and recorded at each temperature as a function of the applied magnetic field.

4.3 RESULTS

For all chalcopyrite samples, two absorption lines were observed. One was broad with a ΔH value between 500 and 700 gauss, depending on the sample composition, while the second was narrower, having a ΔH of approximately 120 gauss for all composition range. It is postulated that the narrow line arises from the Mn^{2+} ions in the ordered structure in the material which is antiferromagnetic in character, while the broad line arises from the Mn^{2+} ions in the disordered structure, which behaves like a spin glass. The intensity of these two lines with respect to each other depends strongly on the relative amount of order and disorder present in each sample. The intensities of these two lines relative to each other are related to the magnitudes of the two peaks observed in $\chi(T)$ measurements, see chapter 3.

In figure (4.3), the derivative of the absorption spectrum at various temperatures is presented for a typical chalcopyrite sample with composition (x=0, y=0.75, z=0.25). From such

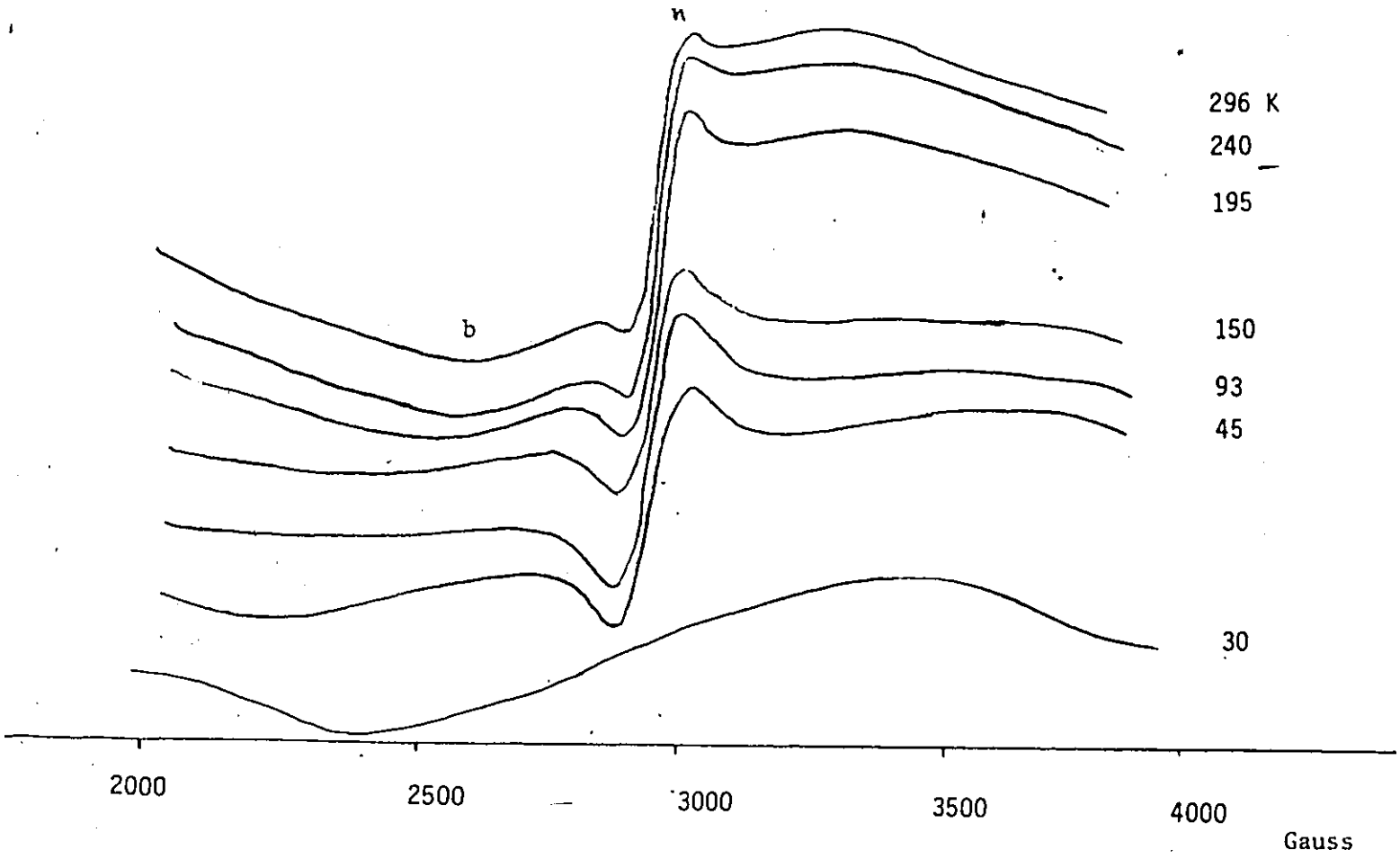

Figure 4.3 Derivative of the absorption spectrum at various temperatures for a chalcopyrite sample with (x=0, y=0.75, z=0.25).

curves the variation of ΔH with temperature for the broad line "b" and the narrow line "n" can be found. The resulting graphs of ΔH vs. T are shown in figure (4.4). ΔH for line "b" starts at a high value and increases relatively slowly at temperatures well above T_g, the spin glass freezing temperature. This behavior is typical of that observed with spin glass material where the value of ΔH is determined mainly by spatial inhomogeneity of the local field seen by the Mn^{2+} atoms and is almost independent of the critical phenomenon at T_g (4). However, the ΔH curve for line "n" shows an almost constant low value until the temperature comes relatively close to the critical transition temperature of 30 ±5 K. It is to be noted that the variation of ΔH for line "n" above 500 gauss is an estimate only since in this range, the peaks corresponding to the two lines coalesce. The form of ΔH for this line is typical of antiferromagnetic behavior, see figure (4.5), i.e. the ordered structure appears to show an antiferromagnetic Néel temperature T_N. This result seems to be in good agreement with the value of 27 K for T_N determined from the magnetic susceptibility measurements for that sample (see chapter 3).

In most of the studied samples with zinc-blende structure, a single symmetric line was observed. The width of this line varies with temperature in the fashion described by figure (4.6). In some of these samples one could clearly identify a second line that has a much smaller ΔH than the first. This narrow line is generally smeared and asymmetric due to its small intensity in comparison to that of the broad line. This asymmetry made the measurement of ΔH for this line very difficult, since the peaks of these lines are not pronounced. Therefore, the values of the ΔH are much less accurate for such lines.

In some samples, chalcopyrite or zinc-blende, a large separation between the zero point and the end of the tail of the derivative curve was found (figure (4.7)). The presence of such a large separation was found to be more persistent in samples that lie on the borderline between the two crystallographic phases, see figure (2.7). Such an effect is attributed to the presence of an absorption line that corresponds to a second phase in the sample. However, this line could not be

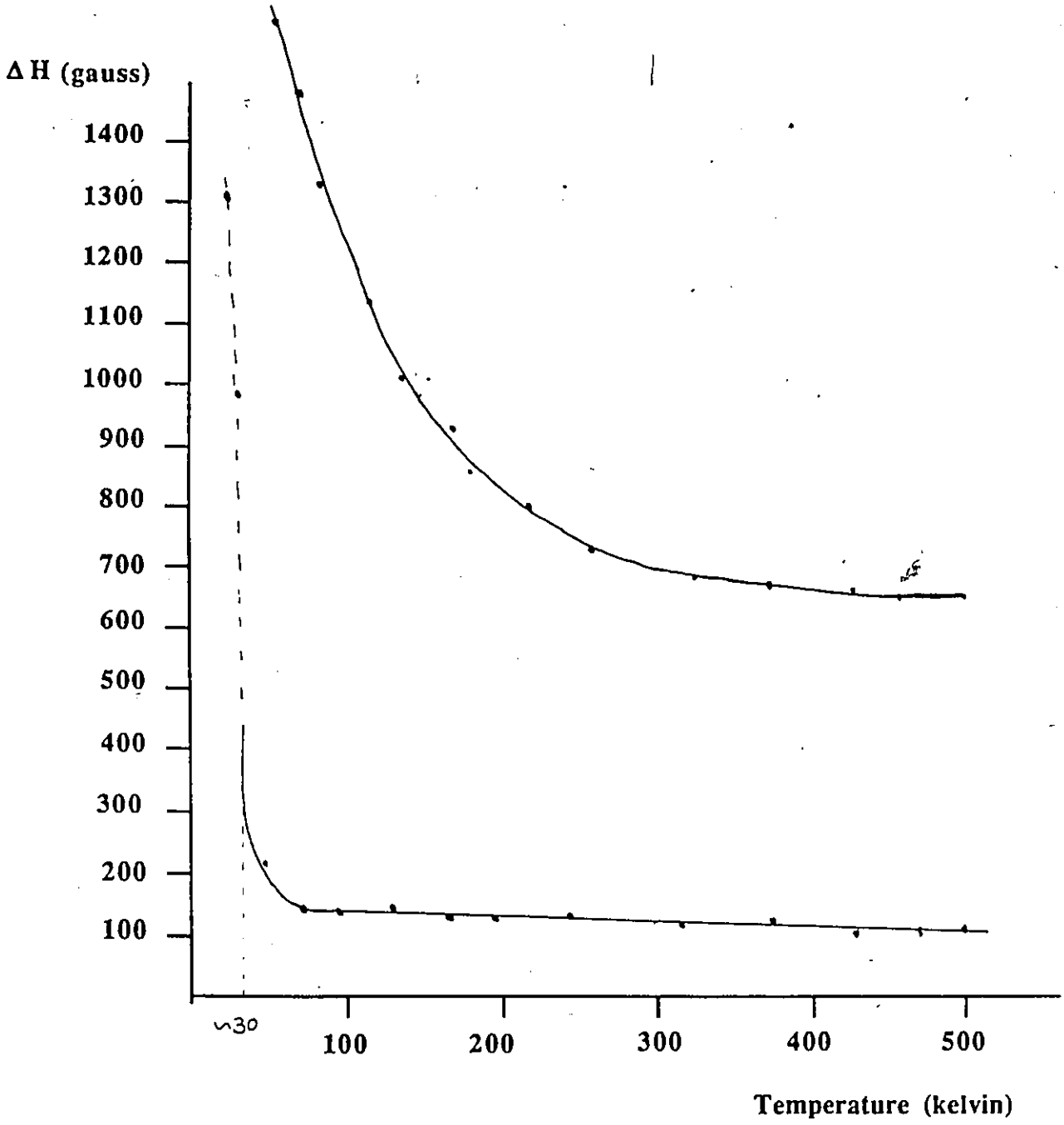

Figure 4.4 Variation of linewidth with temperature for the chalcopyrite sample with (x=0, y=0.75, y=0.25).

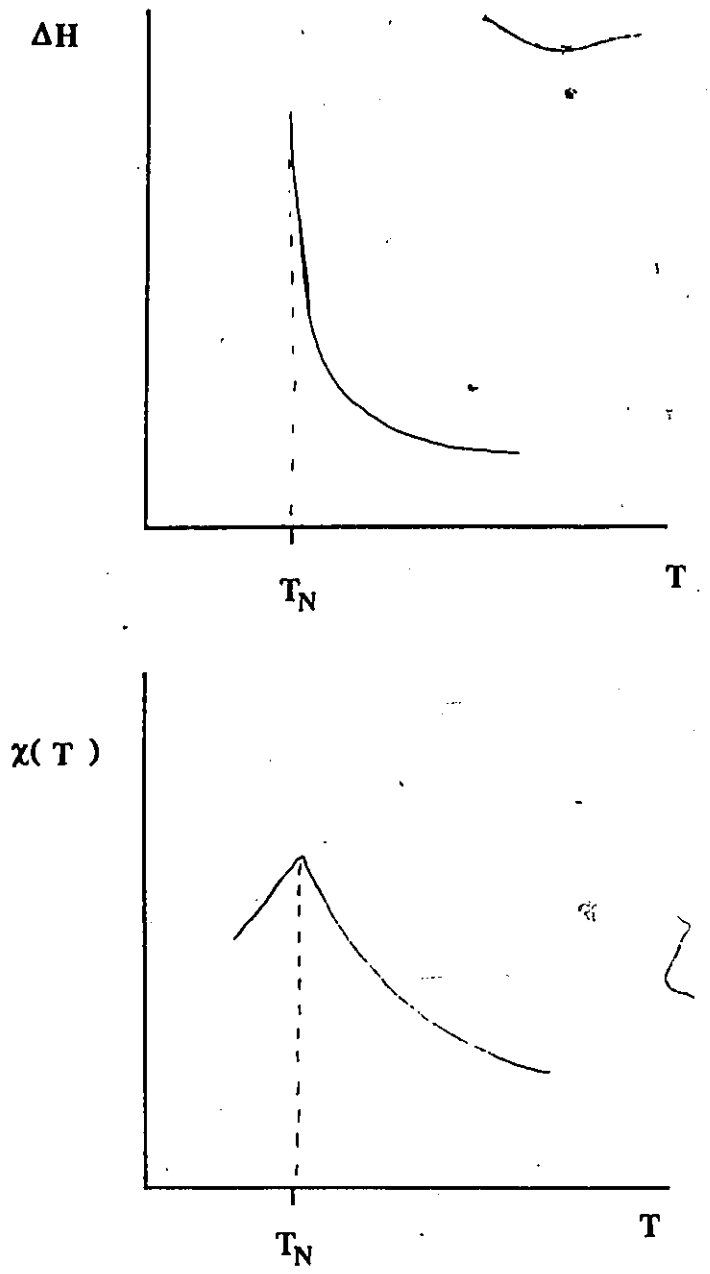

Figure 4.5 Variation of the ESR linewidth and the magnetic susceptibility with temperature for an antiferromagnetic material (Mn F_2), showing a critical phenomenon at T_N

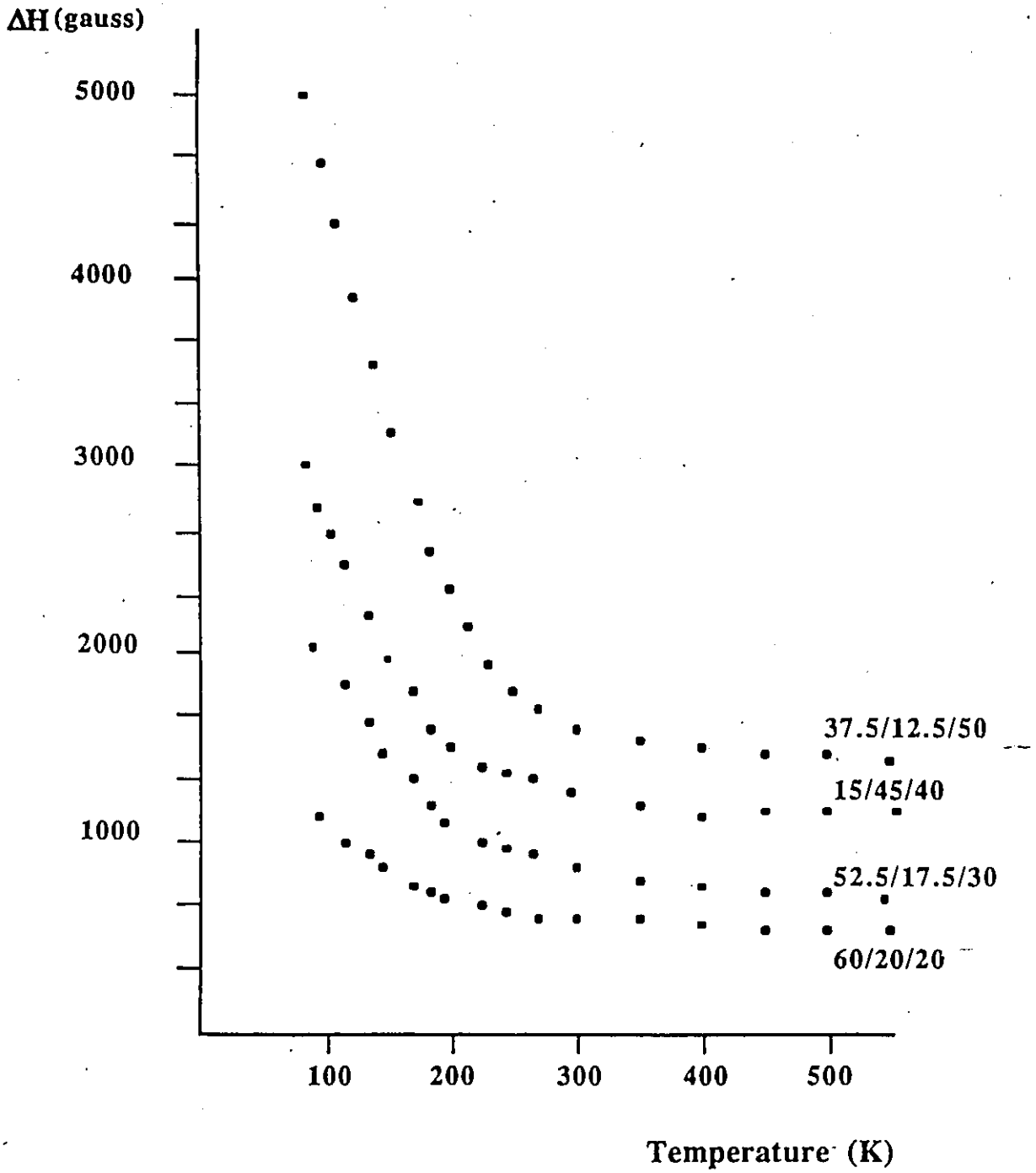

Figure 4.6 Variation of linewidth with temperature for some zinc-blende samples.

seen since its intensity is small and therefore, it becomes masked by the other lines. In cases like this, the analysis of ΔH gave unrealistic results.

Turning back to the effect of order and disorder on the absorption spectrum of the sample, it was observed that the shape and the intensity of the lines depended on the method of cooling from the temperature at which it was annealed, see chapter (2). As mentioned in chapter (2), two methods of cooling were followed: the first is slow cooling, while the other is rapid quenching. The slow cooling results in the presence of two well pronounced lines, see figure (4.8), while in the quenched samples the narrow line becomes very faint and asymmetric. This type of dependence on the method of heat treatment was not very pronounced in the magnetic susceptibility measurements in our alloy system. However, the effect of the cooling method on the $\chi(T)$ was very clear for another alloy system, $Cd_{2x}\,(AgIn)_y\,Mn_{2z}\,Te_2$, studied by this research group. In that case two samples of the same composition (x=0, y=0.75, z=0.25) showed two different behaviors in their $\chi(T)$. In figure (4.9) curve "a" represents one of the samples that has been quenched in water from its annealing temperature and curve "b" represents a sample being cooled slowly by switching the furnace off and leaving the sample to cool over several hours. Curve "a" shows a very strong peak at 8 K and a small one at 24 K, while in "b" the higher temperature peak is strong and the lower temperature peak has almost disappeared (30).

4.4 DETERMINATION OF CURIE-WEISS TEMPERATURE

In the work of Oseroff et. al. on the alloy system $Cd_{1-z}Mn_zTe$ (31), the linewidth of the ESR measurements was assumed to obey the following expression

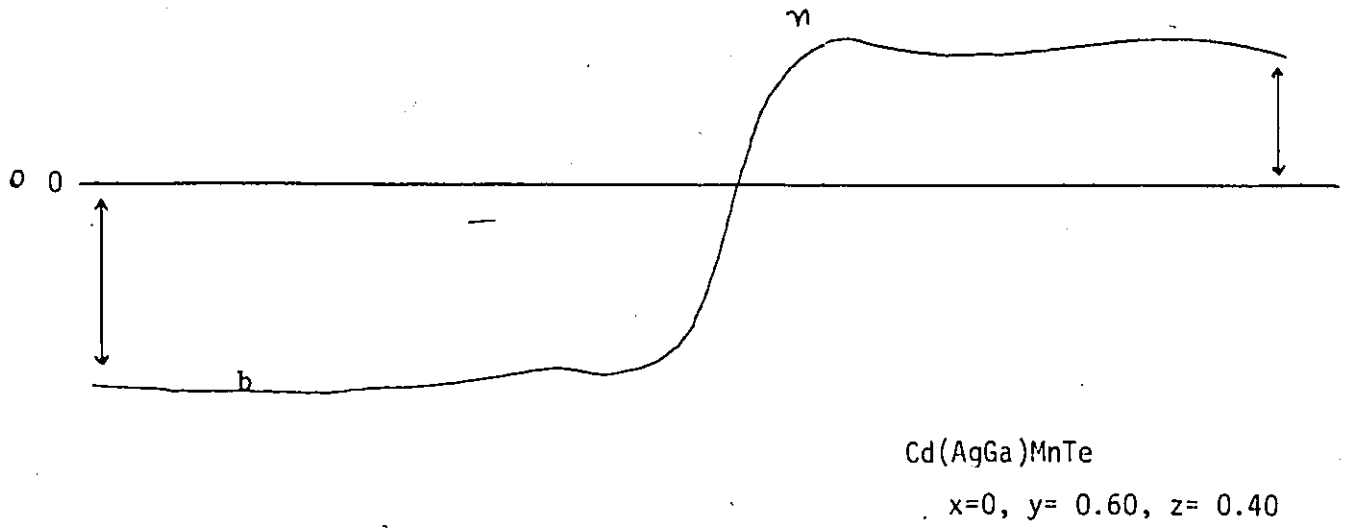

Figure 4.7 Effect of the presence of a second crystallographic phase on the ESR derivative absorption line.

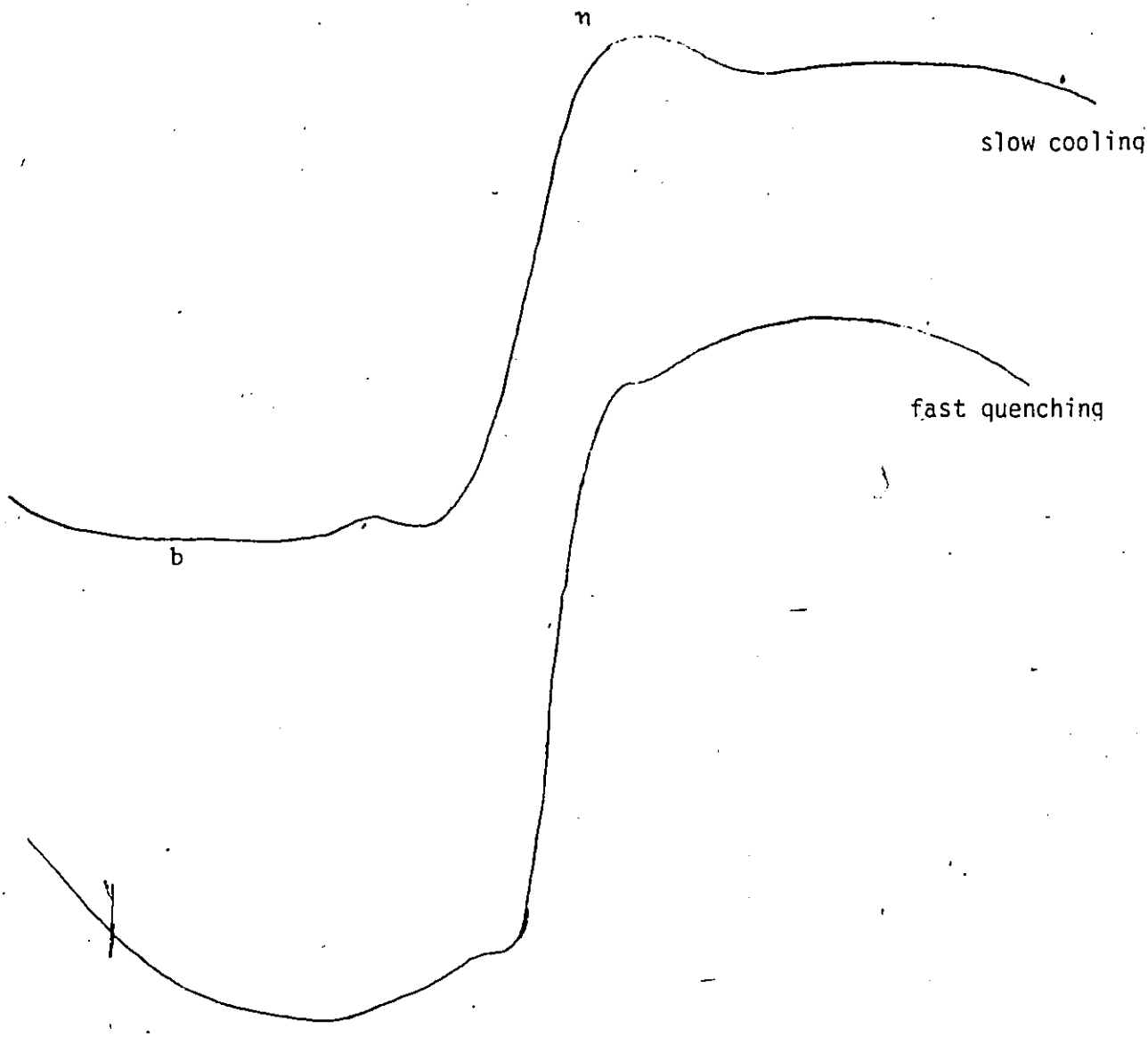

Figure 4.8 Effect of the heat treatment on the relative intensities of the two peaks in the derivative of the absorption line for chalcopyrite sample with (x=0, y=0.65, z=0.35).

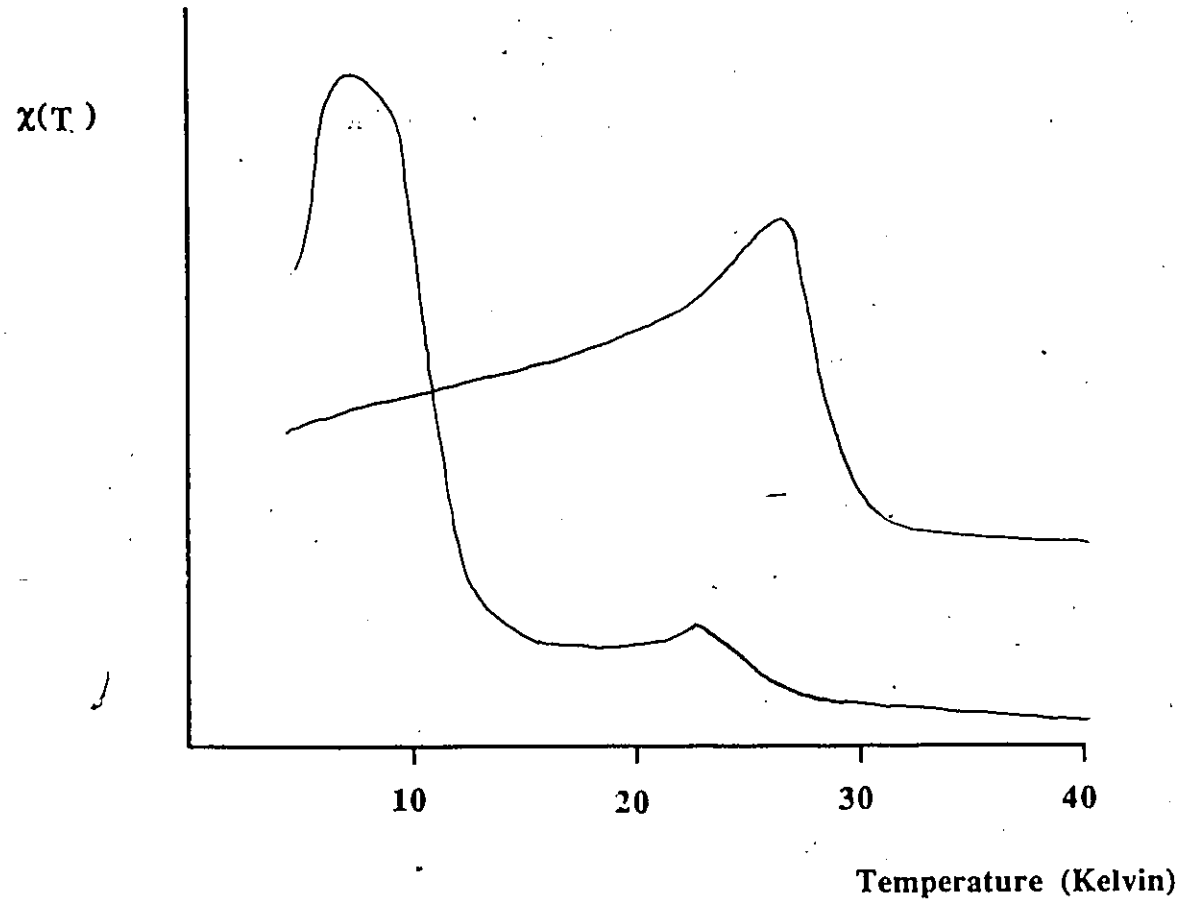

Figure 4.9 Effect of the heat treatment on the intensities of the two peaks observed in the magnetic susceptibility measurements for a sample of the alloy system Cd(AgIn)MnTe with (x=0, y=0.75, z=0.25).

$$\Delta H = A \left(\frac{T_c}{T - T_c}\right)^{\alpha} + B \qquad (4.3)$$

where

B = high temperature linewidth

α = critical exponent

T_c = transition temperature

A = an empirical parameter

which is based on the expression developed by Huber (32) for antiferromagnetic materials above the Néel temperature. Using the analysis of the experimental data, Oseroff found that α and A suffered inconsistent variation with sample composition, in which α could vary by an order of magnitude. Such variation is in contradiction with the fact that α should be independent of composition for the same critical phenomenon. In subsequent work, Oseroff (33,34) modified equation (4.3) giving the following

$$\Delta H = A \left(\frac{T_c}{T - T_c}\right)^{\alpha} + B \left(1 - \frac{\theta}{T}\right) \qquad (4.4)$$

where A and B are empirical parameters independent of temperature, θ is the Curie-Weiss temperature and T_c is the freezing temperature.

However, in our alloy system as well as others (35,36), the ΔH of the broad line (in both zinc-blende and chalcopyrite samples) increased rapidly at temperatures well above the critical temperature T_g that has been determined in chapter (3). Fitting the experimental data in the high temperature region to equation (4.4) gave values of θ consistent with those obtained from measurements of $\chi(T)$. These values were obtained by writing equation (4.4) as

$$T\Delta H = F(T) + B(T - \theta) \qquad (4.5)$$

where F(T) corresponds to the contribution to the linewidth at lower temperatures, and has a negligible contribution at high temperatures. Therefore, from the plot of TΔH vs T at high temperatures, one expects a straight line with an intercept with the temperature axis at θ. Such plots are shown in figures (4.10 a) and (4.10 b) for selected samples. The variation of TΔH with T was found to be linear over a reasonably wide range in the high temperature region. However, at lower temperatures the relation between TΔH and T becomes non-linear due to the contribution of the second term F(T) in equation (4.5).

The application of this type of analysis to the narrow lines in the case of chalcopyrite samples resulted in very small values of θ. For instance, for the sample with composition (x=0, y=0.75, z=0.25), the value of θ is - 50 K (figure (4.11)), while that obtained for the same sample from the measurement of χ(T) is -327 K, see chapter 3. This difference is not yet understood, and is now being investigated by other members of the research group.

As it has been mentioned earlier, in samples lying on the border lines between the two crystallographic phases, one suspects the presence of an absorption line that corresponds to a second phase in the sample. The analysis of TΔH vs T for these samples at high temperatures (figure (4.12)), gave a positive value of θ. These values are unreliable since the measured ΔH does not correspond to a single line but rather to the effect of the combination of several.

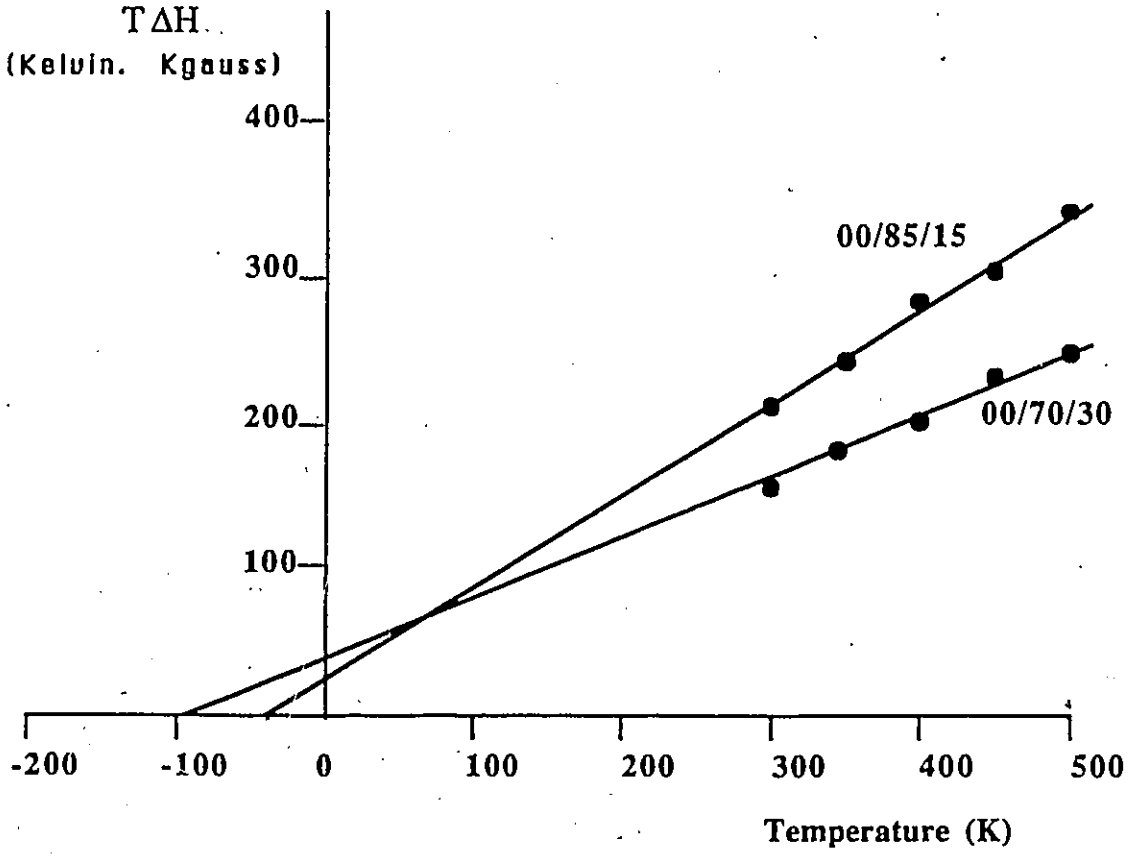

Figure 4.10 a **Fitting of experimental data to equation (4.5) for the disordered line of some chalcopyrite samples.**

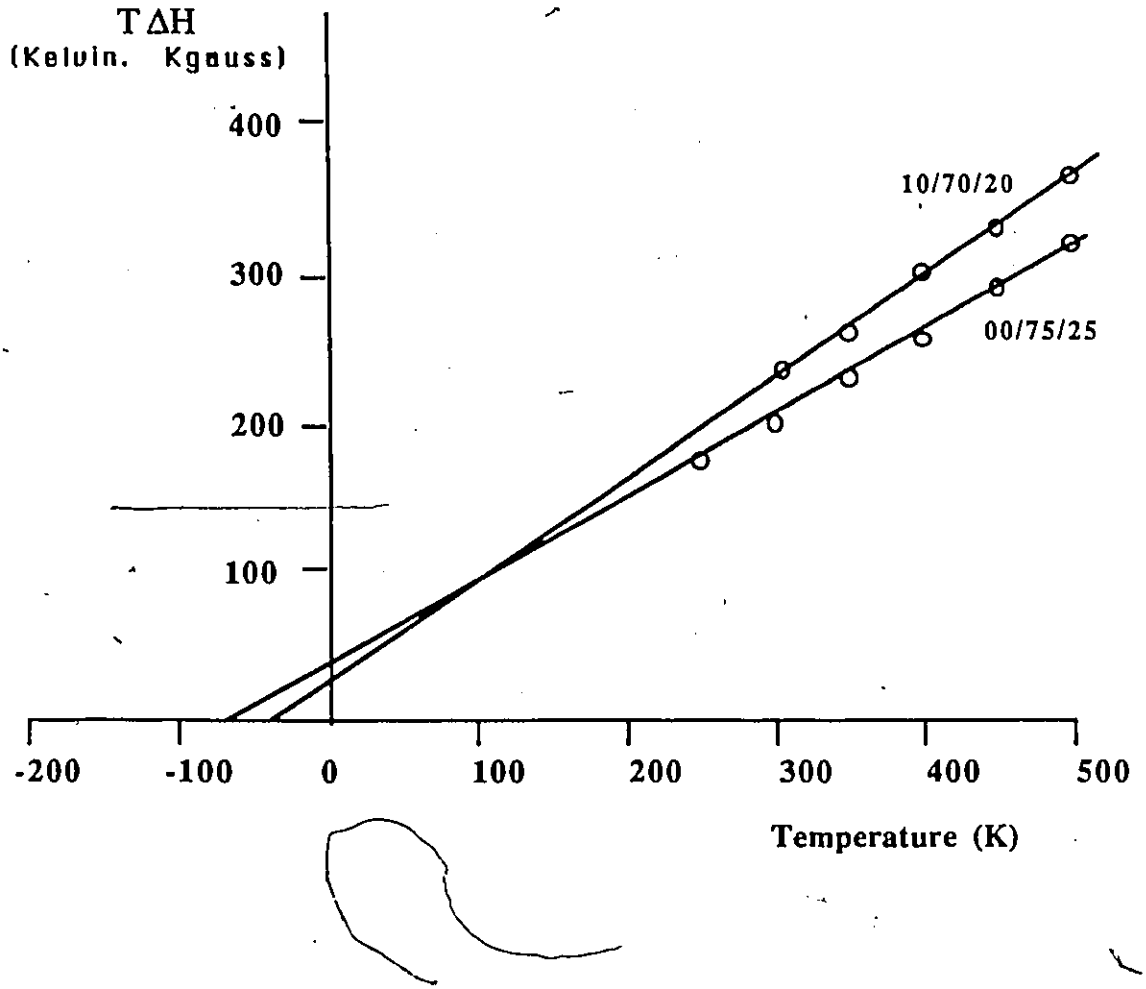

Figure 4.10 b Fitting of experimental data to equation (4.5) for the disordered line of some chalcopyrite samples.

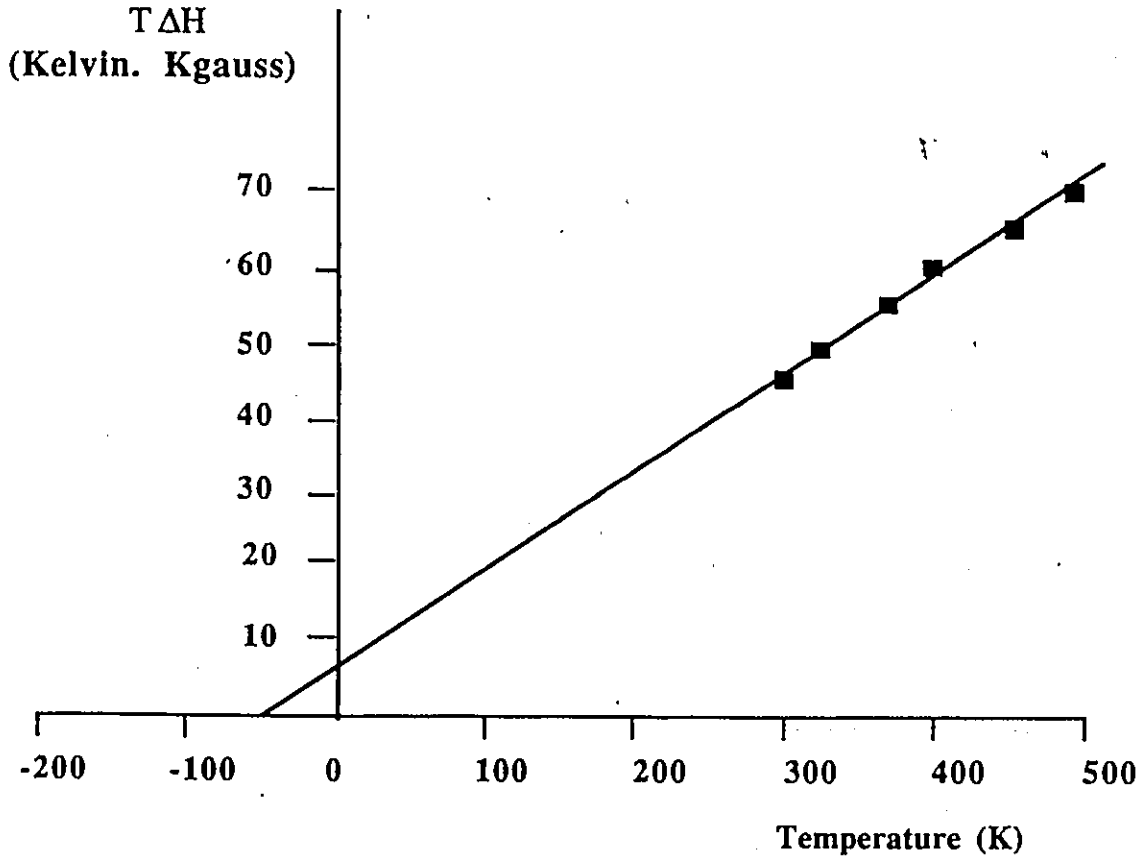

Figure 4.11 Fitting of experimental data to equation (4.5) for the ordered line of a chalcopyrite sample with (x=0, y=.75, z=.25).

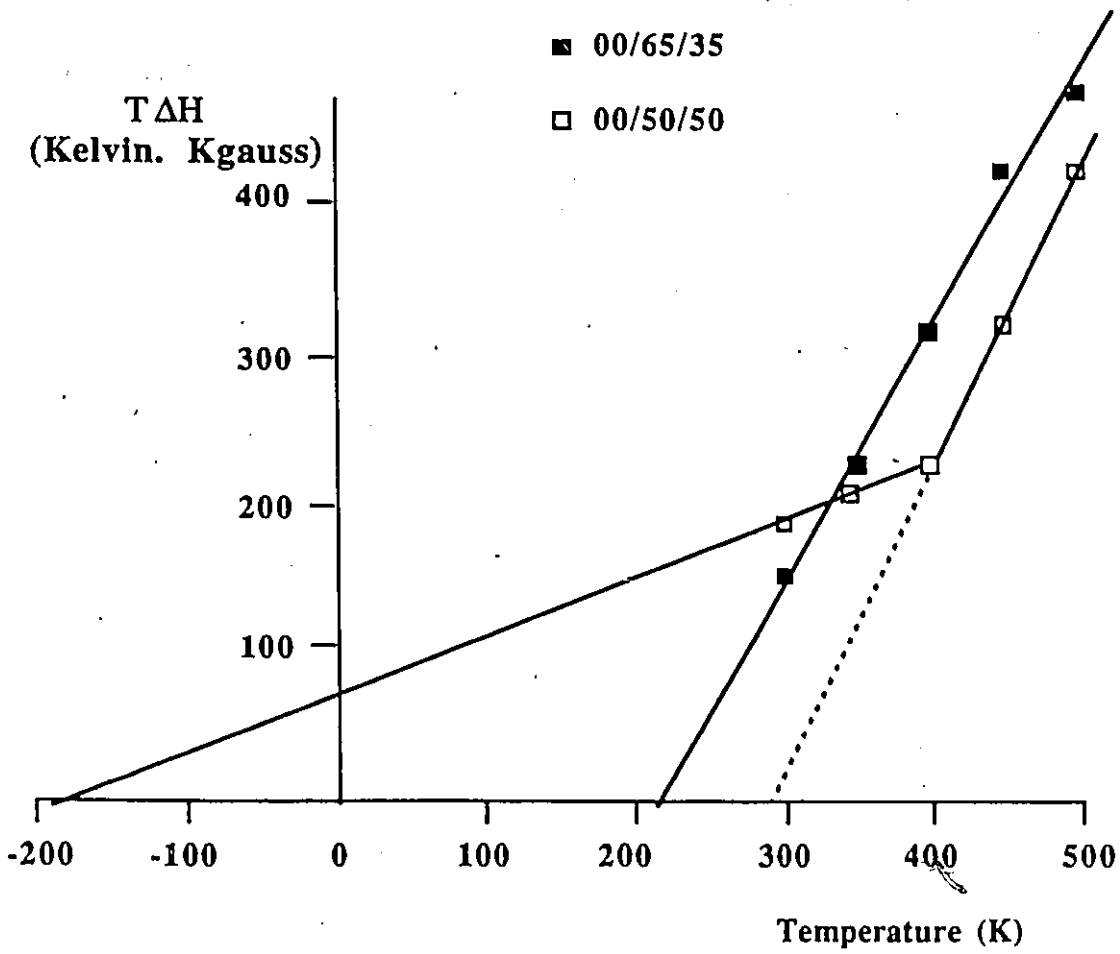

Figure 4.12 Fitting of experimental data to equation (4.5) for chalcopyrite samples suspected of showing two phase behaviour.

CHAPTER 5
OPTICAL ABSORPTION MEASUREMENTS

5.1 INTRODUCTION

Since SMSC materials possess properties of a semiconductor, it is important to investigate their energy gap values. The energy gap of a semiconductor represents the energy difference between the highest point in the valence band and the lowest point in the conduction band. In order to understand the effect of the presence of the magnetic impurities on the value of the energy gap E_g, it is necessary to determine E_g as a function of the concentration of magnetic ions in the material. Also measurements of E_g open a window on the problem of order and disorder in such materials.

Determination of the band gap can be achieved by several methods, of which only two are considered in this work. The first, which is the easiest from the technical point of view, is the optical absorption method. The second is the wavelength modulated reflectance method. The method of optical absorption was used to determine the values of E_g in our alloy system. However, difficulties in the preparation of samples for such measurements limited the number of samples investigated. The main difficulty was to bring the sample to the required thickness in order to get a reasonable transmission of light through it. On the other hand, the impossibility of obtaining good reflecting surfaces on the samples prohibited us from using the wavelength modulated reflectance method. For these reasons, a complete study of the energy gap dependence on sample composition and on the state of order and disorder in the sample could not be realized. However, we were successful in determining E_g for some samples, and these values are in good agreement with those found for similar SMSC alloy systems such as $Cd_{2x}(Ag\ In)_yMn_{2z}Te_2$.

5.2 EXPERIMENT

In semiconductors, two types of interband energy absorption are possible. Transition between extrema of the bands situated at the same point in the Brillouin zone are called direct transitions. If the interband absorption on the other hand takes place between extrema situated at different points in the Brillouin zone, the transition is referred to as indirect.

Direct transition is experimentally characterized by a steep rise in the value of the absorption coefficient as a function of the energy of the incident radiation. The absorption coefficient for a simple parabolic band in the case of an allowed direct transition (37) is given by

$$(\alpha h\nu)^2 = A(h\nu - E_g) \qquad (5.1)$$

where

α is the absorption coefficient

E_g energy gap

A a slowly varying function of $h\nu$

a) Sample Preparation

Samples were cut into small slices with a typical thickness of about 400 μm using a wire saw. The sample was then mounted on an aluminum plate with an aperture in the center which was covered by the sample. The edge and any visible holes in the sample were blocked with silver print. The sample was made as thin as possible by grinding it using 140 μm and 10 μm silica powder. A typical value of sample thickness required in order to obtain a reasonable transmission of light through the sample is of the order of 100 μm. In the case of most samples grown in this work, the slice starts to crack into small pieces during the thinning process at a thickness of

approximately 300 μm due to the brittle nature of these materials. Because of this, the number of experimentally measured values of E_g was greatly limited (we were successful in completing the preparation of only 10 samples out of 32). In the case of the samples that we were not successful in preparing for the absorption method, we tried to polish the sample's surface by etching it with a solution of bromine in 99% pure methanol in order to determine the value of the energy gap using wavelength modulated reflectance method. Unfortunately these measurements could not be completed due to the poor quality of the reflecting surface obtained.

b) Measurements

For sufficiently thick samples, such that no interference effects are observed, the relation between the incident intensity of light on the sample and the transmitted intensity can (37) be written as

$$I = I_o K e^{-\alpha d} \qquad (5.2)$$

where

I_o incident intensity

I transmitted intensity

K a slowly varying function of the incident photon energy

d sample thickness

α absorption coefficient

taking the logarithm of both sides of the equation, we obtain

$$\ln\left(\frac{I}{I_o}\right) = -\alpha d - \ln K \qquad (5.3)$$

In our experiment, α was determined by measuring the incident and the transmitted intensities I_o and I. A tungsten lamp of 40 W with a quartz tube was used as a source. Monochromatic light was obtained by using a Spex 1702 monochromator with a grating blazed at 4 mm. The wavelength was first set in the visible region, and the light coming from the monochromator, see figure (5.1), was focused on the sample. A dielectric filter was placed at the output of the monochromator in order to block the higher orders of short wavelengths present. The sample, as described earlier,was mounted on an aluminum plate suspended in front of the window of a Dumont 6911 photomultiplier. The intensity of the transmitted light detected by this photomultiplier was then fed into a Par 113 roll-off pre-amplifier and then into a Par 186A lock-in amplifier. The lock-in amplifier was locked on the frequency of a chopper placed on the light path before entering the monochromator. The signal from the lock-in was recorded on a chart recorder. The measurement of the transmitted intensity was taken from energies well above E_g to energies well below it. The intensity of the incident light was then measured in the same energy range by removing the sample from the aluminum plate, and therefore measuring the intensity of the light passing through the aperture.

In order to determine the value of α from equation (5.3), it is important to determine the value of ln (K). In our analysis, the value of $\{(1/d) \ln (K)\}$ was considered as part of the "background" and subtracted from the value of $\{(1/d) \ln (I_o/I)\}$. The flat part of the experimental relation between α and the energy of the incident radiation was fitted to a straight line, see figure (5.2 a), and then extrapolated to higher energies. The extrapolated values of $\{(1/d) \ln(I_o/I)\}$ were then subtracted from the measured ones, therefore obtaining the corrected value of α. These values of α were then fitted to equation (5.1) by plotting $(\alpha h\nu)^2$ versus $h\nu$. The straight part of the resulting curve was extrapolated in order to obtain the $h\nu$ intercept, i.e. E_g, see figure (5.2 b).

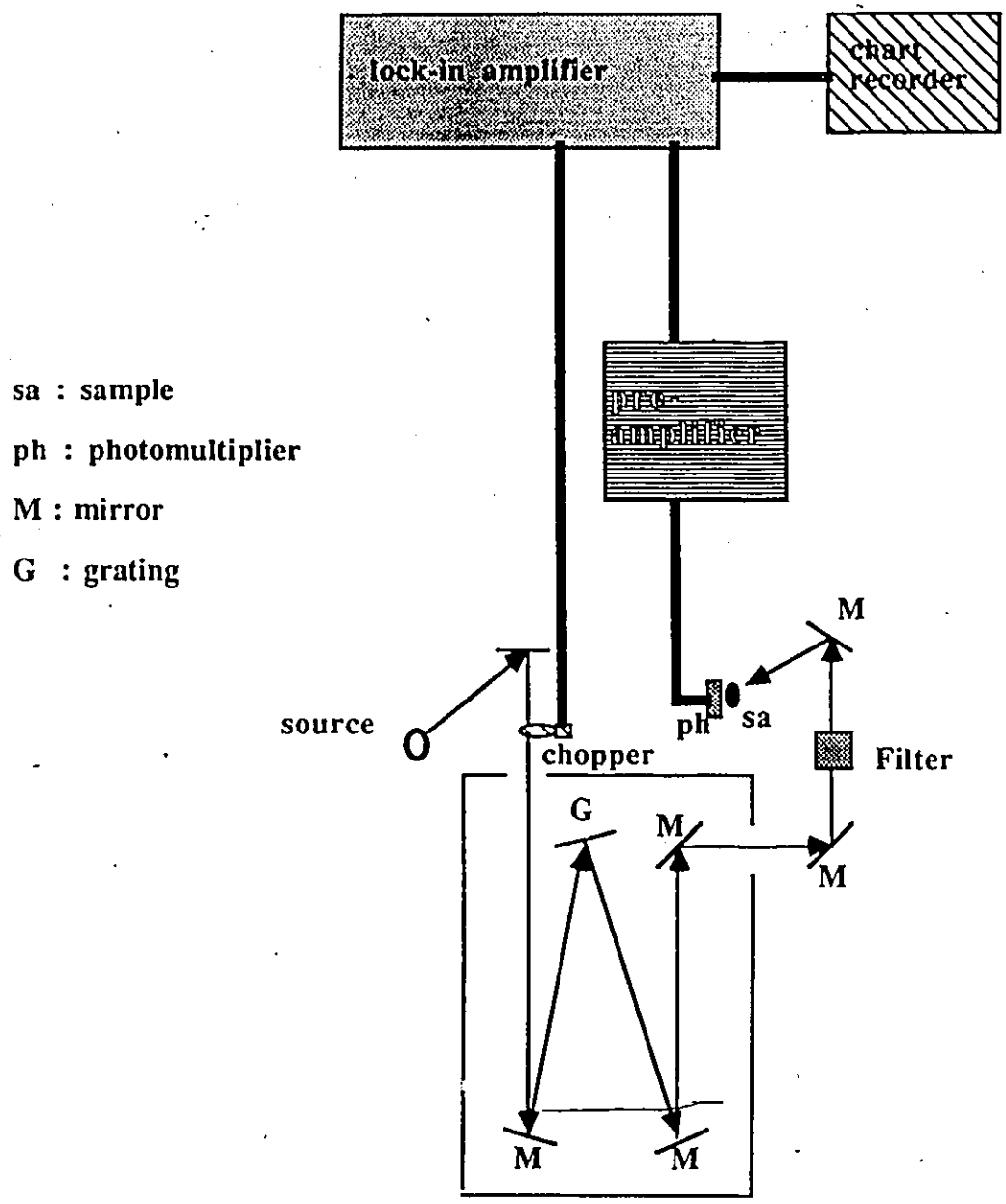

Figure 5.1 Schematic presentation of the experimental setup used in optical absorption measurements.

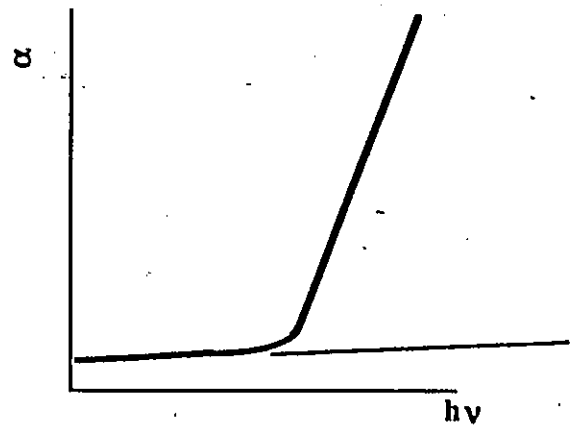

(a)

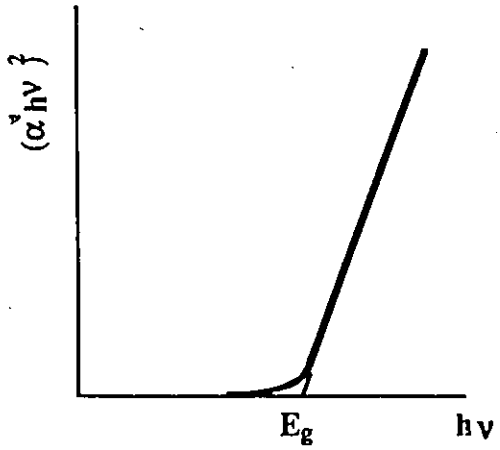

(b)

Figure 5.2 a) Typical variation of the absorption coeficient with incident energy and fitting of the absorption background.
b) Fitting of equation (5.1).

5.3 RESULTS

In figure (5.3), values of E_g for the studied samples are plotted versus manganese concentration. All of the samples presented in this figure are chalcopyrites with x=0. These values were found to be dependent on the method of cooling the samples from the annealing temperature. In this figure, experimental points are divided in three sets, where each represents one type of cooling process. Samples that have been cooled by pulling from the furnace (slow quenching), showed higher values of E_g than those cooled slowly in the furnace (slow cooling) over several hours. In the case of the two samples with composition (x= 0, y= 0.65, z= 0.35) and (x=0, y= 0.60, z= 0.40), two ingots of the sample were treated in two different methods. Rapidly quenched (dropping the sample in cold water from T=500 K) ingots gave values of E_g higher than those obtained from slowly cooled ingots. From these results, no conclusion as to the variation of the samples energy gaps could be arrived at. However, by comparing such results with those obtained by Quintero (6) on $Cd_{2x}(CuIn)_yMn_{2z}Te_2$ (with x=0), one could form an idea regarding the behavior of the samples' optical properties with the method of heat treatment followed in the preparation of the samples. In Quintero's work, three different types of results were obtained corresponding to three different types of lattice structures that the material could assume, see figure (5.4). Chalcopyrite samples in the disordered phase were found to fall on a line that gave an intercept of 2.8 ev when extrapolated to z=1 (this intercept represents the energy gap of MnTe if it would crystallize in the disordered chalcopyrite structure). On the other hand ordered zinc-blende samples fall on a different line giving an intercept of 1.9 ev when extrapolated to z=1, while ordered chalcopyrites give an intercept at 1.35 ev. From figure (5.3) the different extrapolated lines for our alloy system give intercepts that are consistent with those mentioned above. Therefore one could conclude that the lines shown in figure (5.3) represent the same structures present in the alloy system $Cd_{2x}(CuIn)_yMn_{2z}Te_2$. Thus, samples that have been quenched slowly from 650 K have

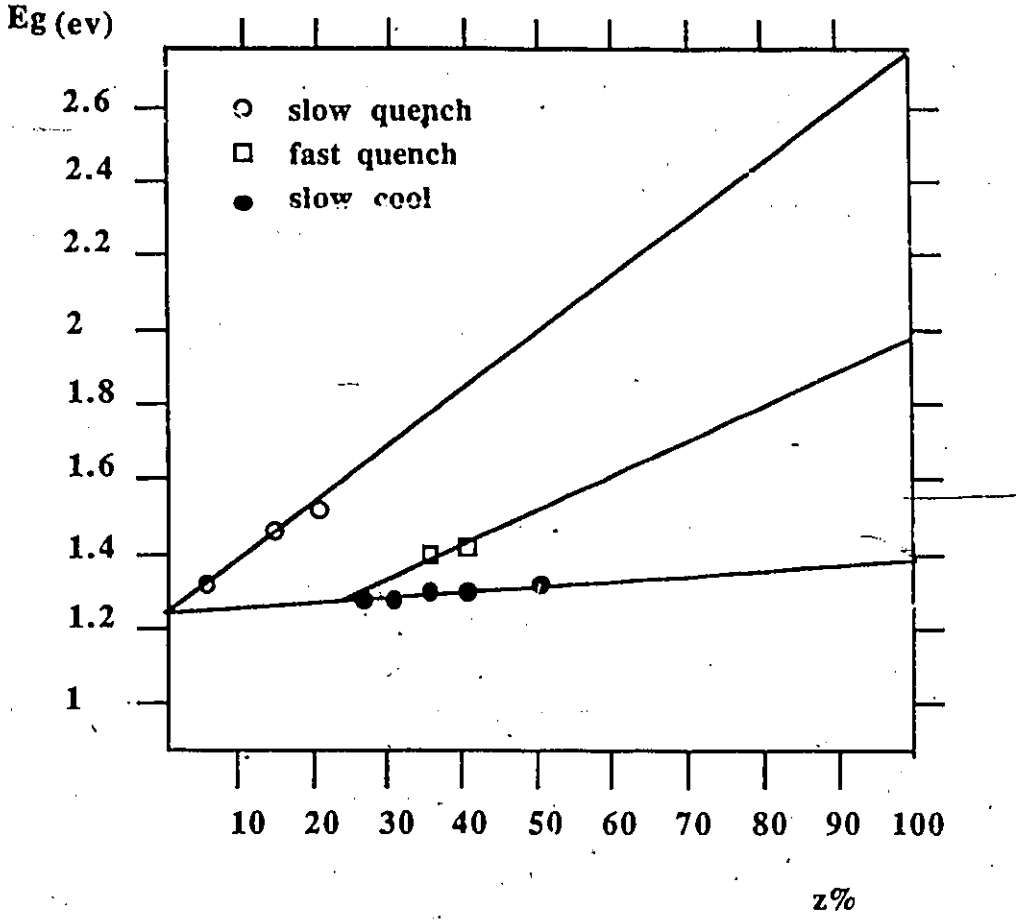

Figure 5.3 Variation of energy gap with concentration for some chalcopyrite samples.

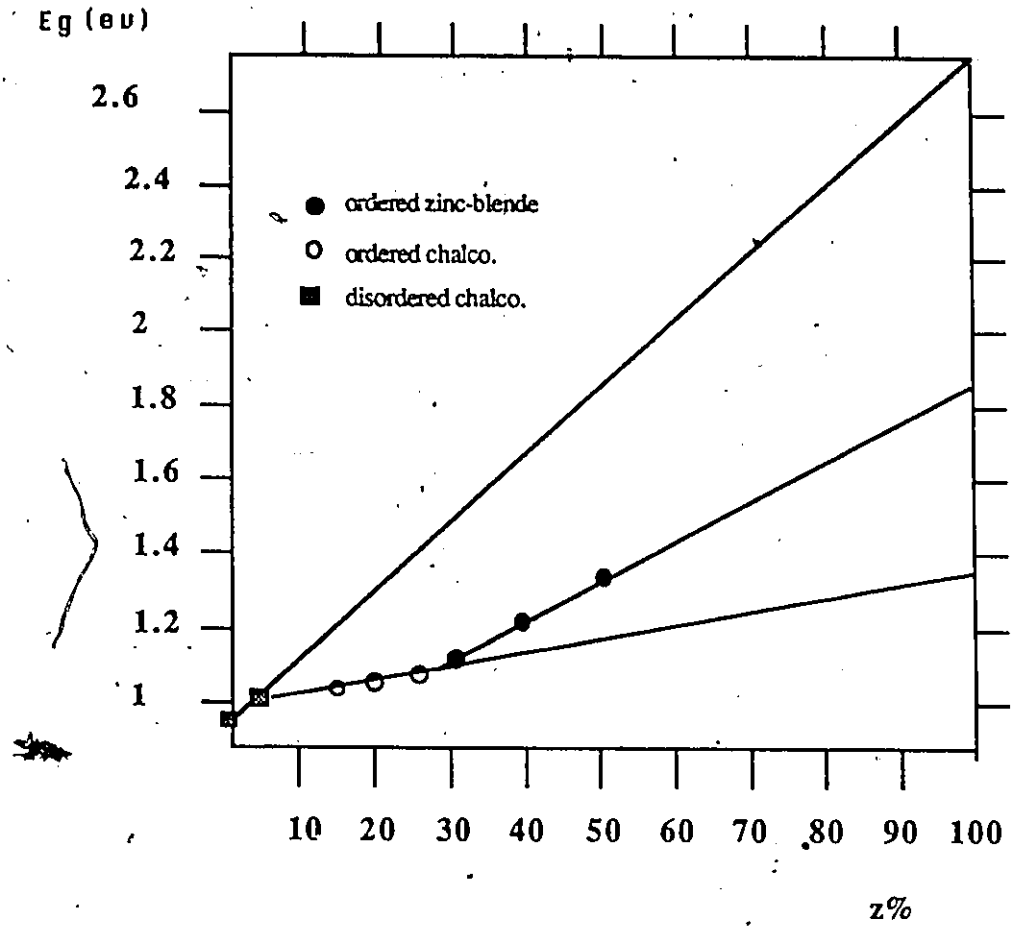

Figure 5.4 Variation of energy gap with manganese concentration for some samples of the alloy system $Cd_{2x}(CuIn)_{y}Mn_{2z}Te_{2}$

disordered chalcopyrite structure and their energy gap values are higher than the values they would have if they were in an ordered chalcopyrite structure. The presence of the ordered zinc-blende samples arises from the fact that these samples are quenched from 500 K, where the samples crystallize in the zinc-blende structure if we consider a phase diagram similar to that proposed by Aresti et al.(27) in the case of the alloy system $(CuIn)_{1-z}Mn_{2z}Te_2$ (see chapter 3).

CONCLUSION

Some properties of the pseudo-ternary alloy system $Cd_{2x}(AgGa)_yMn_{2z}Te_2$ have been presented, including lattice structures and lattice constants, d.c magnetic susceptibility, ESR linewidth and energy gap values using an optical absorption method.

From the powder x-ray diffraction measurements, samples were found to crystallize in one of two possible crystal structures depending on composition. The first of these two structures is the adamantine zinc-blende structure, which extends over a wide range of composition. The second is the body centered tetragonal chalcopyrite structure.

In most of the zinc-blende samples studied, measurements showed a single pronounced cusp in the variation of magnetic susceptibility with temperature (at a temperature T_g). This cusp is attributed to the random freezing of the spins in the alloy which undergoes a paramagnetic to spin glass transition at T_g. In most of chalcopyrite samples, two cusps were observed. It is postulated that such behavior results from the existence of two magnetic phases in the material. The first of these two phases is the disordered phase in which the magnetic ions are randomly distributed on the lattice sites, and which shows a spin glass freezing temperature T_g. The second phase represents the antiferromagnetic ordering of the spins on one of the sublattices of the structure, showing a critical phenomenon at the Néel temperature T_N. The relative intensities of the observed two peaks were found to depend on the exact method of heat treatment of the sample.

From ESR measurements, most of zinc-blende samples showed a single absorption line. Analysis of the linewidth indicates that this line behaves in a fashion typical of that of spin glass materials. In most of the chalcopyrite samples studied, two absorption lines were observed. From the analysis of the linewidth of these lines it was found that the two lines represent the ordered and the disordered magnetic phases.

Optical absorption measurements were carried out in order to determine the energy gap of these materials. Due to difficulties in the sample preparation, a complete study of the dependence of the energy gap on composition was not achieved. However, from the few experimental data obtained, it was found that the energy gap of the sample depends on whether the magnetic ions in the sample are ordered or disordered. Such dependence of the energy gap on the ordering of the magnetic ions was found to be similar to that observed in other SMSC alloy systems such as $(Cd_{2x}(CuIn)_yMn_{2z}Te_2)$.

Unfortunately, due to the insensitivity of the x-ray diffraction measurements to the presence of the order and disorder in the material, information regarding the exact type of ordering of the magnetic ions in the lattice could not be obtained. To obtain such information, neutron diffraction measurements are being made by another member of our research group.

The experimental data obtained from the magnetic susceptibility measurements were fitted to the theoretical model of superexchange proposed by Geertsma et al. In this model, the interactions between the manganese ions take place via virtual transitions between the valence band and the $3d^5$ energy levels of the Mn^{2+} ions. The theoretically predicted values of the Curie-Weiss temperature (θ) from this model were found to agree, within the experimental error, with the experimental values. An additional contribution to the exchange interaction between the ions may be present due to the Bloembergen-Rowland type of interaction mechanism. In this mechanism, interactions between the magnetic ions take place via virtual transitions between the valence and conduction bands. Calculation of the magnitude of this contribution could not be obtained due to the lack of a complete set of experimental data on the energy gap values as a function composition required for such calculation, but other results indicate that for the present alloys, the Bloembergen-Rowland contribution should not exceed 10% of the total.

REFERENCES

1-J.K. Furdyna, J. Appl. Phys. 53 7637 (1982)

2- J.A. Gaj, J. Appl. Phys. Soc., Japan 49 797 (1980)

3- N.B. Brandt and V.V.Moshchalkov, Adv. Phys. 33 no.3, 193 (1984)

4- T. Donofrio, Ph.D. thesis, University of Ottawa (1986)

5- D. Beckett, Master's thesis, University of Ottawa (1986)

6- M. Quintero, Ph.D. thesis, University of Ottawa (1985)

7- B. Coles, from "Amphorous magnetism", (Plenum, N.Y. 1973)

8- K. Binder, "Fundamental problems in statistical mechanics", (North Holland, Amsterdam).

9- D. Chodhury and A. Mookerjee, Phys. Rep. 114, No. 1 (1984), p 1-98

10- P. I. Ford, Contemp. Phys. 23, 141, (1982)

11- J. L. Tholence and R. Tournier, J. Phys. (Paris) 35, c4 (1974), 229

12- J. L. Tholence and R. Tournier, Physica 86-88B (1977), 852

13- A. P. Murani, J. Magn. Mag. Mat. 5, (1977), 95

14- F. Hartmann-Boutron, J. Phys. Lett. (Paris), 43 (1982) L853

15- M. Esporne and A. Mauger, Phys. Rev. 25B 4674 (1982)

16- J. Ginter, J. Kossut, L. Swierkowoski, Phys. Stat. Sol. (b) 96, 735 (1979)

17- G.S. Grest, E.G. Gable, Phys. Rev. Lett. 1 43, 1182, (1979)

18- M.F. Sykes, J.W. Essam, Phys. Rev. 133. A310 (1964)

19- B.E. Larson, K.C. Haas, H. Ehrenreich, A.E. Carlsson, Solid State Commun. 56, 347 (1985)

20- M. Escorne and A. Mauger, Phys. Rev. B107, 309 (1980)

21- W. Geertsma, C. Haas, G.A. Sawatzky, Physica 86-88 B (1977) 1039

22- J.C. Woolley, S.F. Chehab, T. Donofrio, S. Manhas, G. Lamarche and A. Manoogian, J. Magn. Mag. Mat. 61 (1986) 13-20

23- J.S. Smart, "Magnetism" vol.III, edition G.T. Rado and H. Shul (AP, N.Y., 1963)

24- N. Bloembergen and T.J. Rowland, Phys. Rev. 97 (1955) 1679

25- T. Donofrio, G. Lamarche and J.C. Woolley, J. Appl. Phys. 57, (1985) 1932

26- C. Lewiner, J. Gaj and G. Bastard, . Phys. 41 (1980) c5-289

27- A. Aresti, L. Garbato, G. Lehmann and P. Manca, " presented at the International Conference on Ternary and Multenary Compounds, september 1986, Colorado" _ Proceedings are to be Published.

28- A.H. Morrish, " The physical principle of magnetism", Robert Krieger Publishing Company, (1960).

29- S. Chehab, Ph.D. thesis, University of Ottawa, 1986

30- J.C. Woolley, G. Lamarche, A. Manoogian, M. Quintero, L. Dierker, M. Al-Najjar, D. Proux, C. Neal and R. Goudreault, " presented at the International Conference on Ternary and Multenary Compounds, september 1986, Colorado" _ Proceedings are to be Published.

31- S. Oseroff, R. Calvo and W. Giriat, J. Appl. Phys. 50, 7738 (1979)

32- D.L. Huber, Phys. Rev. B6, 3180 (1972)

33- S. Oseroff, Phys. Rev. B25, 6584 (1982)

34- S. Oseroff, R. Calvo, z. Fisk, F. Acker, Phys. Lett. 80A, 311 (1980)

35- S. Chehab, J.C. Woolley, A. Manoogian and G. Lamarche, J. Magn. Mag. Mat., 62 (1986) 312-324

36- A. Manoogian, B.W. Chan, R. Brun del Re, T. Donofrio, J.C. Woolley, J. Appl. Phys. 53, (12) (1982)

37- D.L. Greenway and G. Harbeke, "Optical properties of Semiconductors", Pergamon Press, N.Y., 1968